Earth and Planetary Science Letters 301 (2011) 241–255

Contents lists available at ScienceDirect

Earth and Planetary Science Letters

journal homepage: www.elsevier.com/locate/epsl

The Lhasa Terrane: Record of a microcontinent and its histories of drift and growth

Di-Cheng Zhu [a,*], Zhi-Dan Zhao [a], Yaoling Niu [a,b,c], Xuan-Xue Mo [a], Sun-Lin Chung [d], Zeng-Qian Hou [e], Li-Quan Wang [f], Fu-Yuan Wu [g]

[a] State Key Laboratory of Geological Processes and Mineral Resources, and School of Earth Science and Resources, China University of Geosciences, Beijing 100083, China
[b] Department of Earth Sciences, Durham University, Durham DH1 3LE, UK
[c] School of Earth Sciences, Lanzhou University, Lanzhou 730000, China
[d] Department of Geosciences, National Taiwan University, Taipei 106, China
[e] Institute of Geology, Chinese Academy of Geological Sciences, Beijing 100037, China
[f] Chengdu Institute of Geology and Mineral Resources, Chengdu 610082, China
[g] Institute of Geology and Geophysics, Chinese Academy of Sciences, Beijing 100029, China

A R T I C L E   I N F O

Article history:
Received 15 May 2010
Received in revised form 30 October 2010
Accepted 2 November 2010
Available online 26 November 2010

Editor: T.M. Harrison

Keywords:
zircon U–Pb dating and Hf isotope
Mesozoic–early Tertiary magmatic rocks
lithospheric architecture
tectonomagmatic evolution
Lhasa Terrane
Tibet

A B S T R A C T

The Lhasa Terrane in southern Tibet has long been accepted as the last geological block accreted to Eurasia before its collision with the northward drifting Indian continent in the Cenozoic, but its lithospheric architecture, drift and growth histories and the nature of its northern suture with Eurasia via the Qiangtang Terrane remain enigmatic. Using zircon *in situ* U–Pb and Lu–Hf isotopic and bulk-rock geochemical data of Mesozoic–Early Tertiary magmatic rocks sampled along four north–south traverses across the Lhasa Terrane, we show that the Lhasa Terrane has ancient basement rocks of Proterozoic and Archean ages (up to 2870 Ma) in its centre with younger and juvenile crust (Phanerozoic) accreted towards its both northern and southern edges. This finding proves that the central Lhasa subterrane was once a microcontinent. This continent has survived from its long journey across the Paleo-Tethyan Ocean basins and has grown at the edges through magmatism resulting from oceanic lithosphere subduction towards beneath it during its journey and subsequent collisions with the Qiangtang Terrane to the north and with the Indian continent to the south. Zircon Hf isotope data indicate significant mantle source contributions to the generation of these granitoid rocks (e.g., ~50–90%, 0–70%, and 30–100% to the Mesozoic magmatism in the southern, central, and northern Lhasa subterranes, respectively). We suggest that much of the Mesozoic magmatism in the Lhasa Terrane may be associated with the southward Bangong–Nujiang Tethyan seafloor subduction beneath the Lhasa Terrane, which likely began in the Middle Permian (or earlier) and ceased in the late Early Cretaceous, and that the significant changes of zircon $\varepsilon_{Hf}(t)$ at ~113 and ~52 Ma record tectonomagmatic activities as a result of slab break-off and related mantle melting events following the Qiangtang–Lhasa amalgamation and India–Lhasa amalgamation, respectively. These results manifest the efficacy of zircons as a chronometer (U–Pb dating) and a geochemical tracer (Hf isotopes) in understanding the origin and histories of lithospheric plates and in revealing the tectonic evolution of old orogenies in the context of plate tectonics.

1. Introduction

The Tibetan Plateau is a geological amalgamation of several continental collision events since the Early Paleozoic (cf. Dewey et al., 1988; Kapp et al., 2007; Yin and Harrison, 2000; Zhu et al., 2009a, 2010). The Lhasa Terrane is the southernmost Eurasian block speculated as having rifted from Gondwana in the Triassic or the mid- to late Jurassic and drifted northward across the Tethyan Ocean basins before it collided with Eurasia along the Bangong–Nujiang suture (BNSZ; Fig. 1a) in the Cretaceous (earlier in the east and later in the west) (cf. Audley-Charles, 1983, 1984, 1988; Dewey et al., 1988; Kapp et al., 2007; Matte et al., 1996; Metcalfe, 2010; Sengör, 1987; Yin and Harrison, 2000; Zhang et al., 2004), and as having an Andean-type active continental margin in the south prior to the collision with the northward moving Indian continent in the Cenozoic marked by the Indus–Yarlung–Zangbo suture (IYZSZ; Fig. 1a) (e.g., Aitchison et al., 2007; Mo et al., 2008; Rowley, 1996; Yin and Harrison, 2000). However, the lithospheric architecture of the Lhasa Terrane (e.g., the age, composition and spatial distribution of crustal lithologies) and the nature of its northern suture (BNSZ) with Eurasia via the Qiangtang Terrane remain poorly understood. Geological studies in this regard have been hampered by complex crustal deformation as a result of continued convergence of the Indian lithosphere against the Lhasa Terrene through underthrusting (e.g., Kosarev et al., 1999). For example, despite much research on the Mesozoic geology of the Lhasa

* Corresponding author. State Key Laboratory of Geological Processes and Mineral Resources, China University of Geosciences, 29# Xue-Yuan Road, Haidian District, Beijing 100083, China. Tel.: +86 10 8232 2094; fax: +86 10 8232 2094.
E-mail address: dchengzhu@163.com (D.-C. Zhu).

0012-821X/$ – see front matter
doi:10.1016/j.epsl.2010.11.005

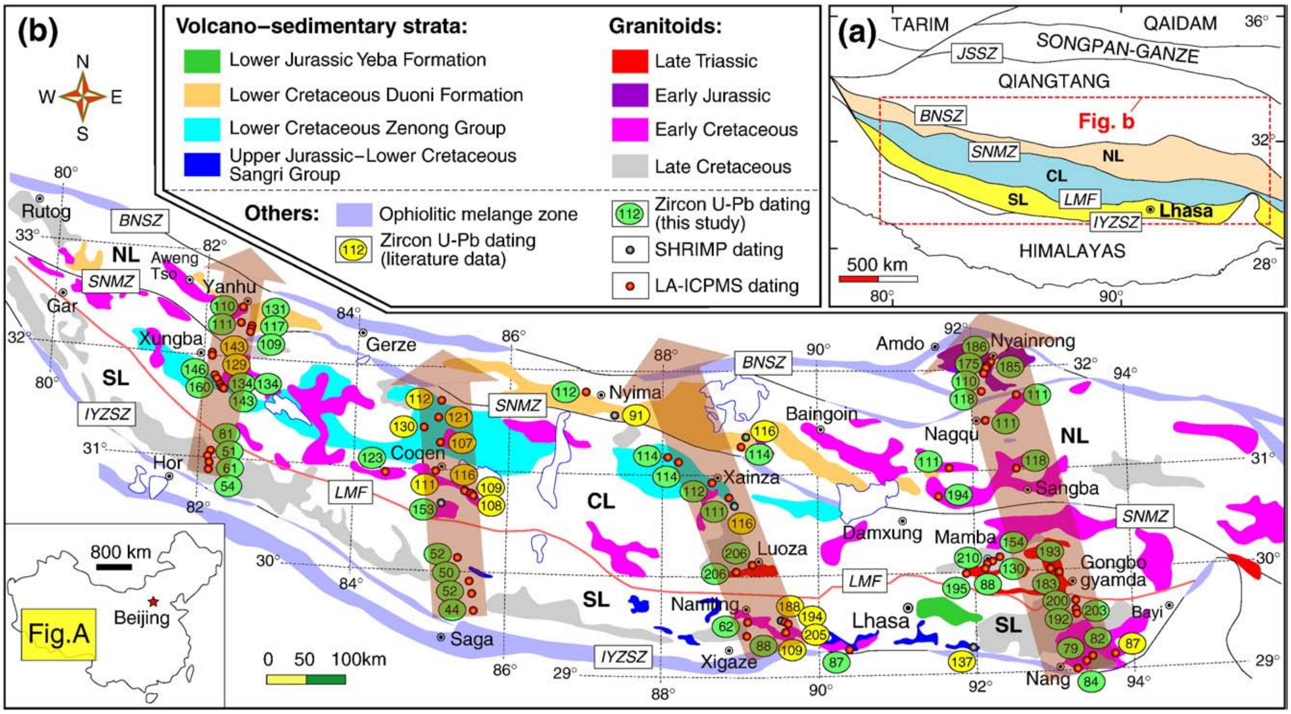

Fig. 1. Tectonic framework of the Tibetan Plateau and the Lhasa Terrane. (a) Showing the Lhasa Terrane in the context of the Tibetan Plateau. (b) The geology of the Lhasa Terrane where four north–south sampling traverses of Mesozoic–early Tertiary magmatic rocks are indicated by sample locations aided by shaded bands with arrows. The ovals with numerals give crystallization ages in Ma using *in situ* zircon U–Pb dating techniques (see supplementary online data for analytical details). Abbreviations: JSSZ = Jinsha suture zone; BNSZ = Bangong–Nujiang suture zone; SNMZ = Shiquan River–Nam Tso Mélange Zone; LMF = Luobadui–Milashan Fault; IYZSZ = Indus–Yarlung Zangbo Suture Zone. SL = southern Lhasa subterrane, CL = central Lhasa subterrane, NL = northern Lhasa subterrane.

Terrane, the basement rocks are only found in the Amdo and SW Nyainqêntanglha Ranges (Dewey et al., 1988; Guynn et al., 2006; Hu et al., 2005; Xu et al., 1985), and the origin of the extensive Mesozoic magmatism continues in dispute (Chiu et al., 2009; Chu et al., 2006; Coulon et al., 1986; Harris et al., 1990; Ji et al., 2009a; Kapp et al., 2005, 2007; Pearce and Mei, 1988; Zhang et al., 2010a; Zhu et al., 2009b, c). Seismic tomography is useful, but it can only tell us the present-day snapshot of the lithosphere architecture (Kosarev et al., 1999; McKenzie and Priestley, 2008; Royden et al., 2008), providing no information on material histories.

The recent analytical advances that combine *in situ* U–Pb dating and Hf-isotope analysis on zircons (Kemp et al., 2006; Scherer et al., 2007) from magmatic rocks make it possible to unravel the nature, history, and lithosphere architecture of the Lhasa Terrane. Zircons, which are abundant in the more felsic magmatic rocks, can provide precise crystallization ages of the host magmas (i.e., U–Pb dating) and can also tell whether the host magmas result from remelting of the ancient mature crustal materials or involve newly-derived mantle material for net crustal growth (i.e., Hf isotope tracer) (Griffin et al., 2002; Kemp et al., 2006; Scherer et al., 2007). Importantly, their physiochemical resistance allows zircons to survive from subsequent geological events. As a result, zircons can record information on their geological histories and have thus become a powerful tracer for studying crustal evolution (Kemp et al., 2006; Scherer et al., 2007).

In this paper, we report a combined *in situ* U–Pb dating and Hf-isotope analysis on zircons from Mesozoic–early Tertiary magmatic rocks sampled along four north–south traverses across the Lhasa Terrane (Fig. 1b). These new data, together with the data in the recent literature (Ji et al., 2009a; Zhang et al., 2010a; Zhou et al., 2008; Zhu et al., 2009b, c), enable us to offer unprecedented perspectives on the lithospheric architecture of the Lhasa Terrane, its tectonomagmatic evolution histories and crustal growth in the context of the plate tectonics thanks to the efficacy of zircons in magmatic rocks as a chronometer (U–Pb dating) and geodynamic tracer (Hf isotopes).

2. Mesozoic–Early Tertiary magmatism in the Lhasa Terrane and samples

The Lhasa Terrane is one of the four huge W–E trending tectonic belts (i.e., the Songpan–Ganzi belt, Qiangtang, Lhasa and the Himalaya) of the Tibetan Plateau (Fig. 1a). According to different sedimentary cover rocks, it can be divided into northern, central, and southern subterranes, separated by the Shiquan River–Nam Tso Mélange Zone (SNMZ) and Luobadui–Milashan Fault (LMF), respectively (Figs. 1a–b). Apart from the widespread Cretaceous–early Tertiary Gangdese batholiths and Linzizong volcanic succession that have been known for decades in the southern Lhasa subterrane (Coulon et al., 1986; Harris et al., 1990; Ji et al., 2009a; Lee et al., 2009; Mo et al., 2007, 2008; Pearce and Mei, 1988; Wen et al., 2008), abundant Mesozoic magmatic rocks (though poorly dated) are also present in the central and northern Lhasa subterranes (Fig. 1b) (Chiu et al., 2009; Chu et al., 2006; Coulon et al., 1986; Guynn et al., 2006; Harris et al., 1990; Zhu et al., 2008a, 2009a).

In the southern Lhasa subterrane, the sedimentary cover is limited, mainly of Late Triassic–Cretaceous age (Pan et al., 2006; Zhu et al., 2008b). The known Mesozoic volcanic rocks in this subterrane include mafic and silicic varieties of the Lower Jurassic Yeba Formation (190–175 Ma) (Zhu et al., 2008b) and adakite-like andesitic rocks of the Upper Jurassic–Lower Cretaceous Sangri Group (Zhu et al., 2009c) (Fig. 1b). Recent zircon U–Pb age results indicate that the Mesozoic plutonic rocks in this subterrane were emplaced over a long time period from the Late Triassic (ca. 205 Ma) to Late Cretaceous (ca. 72 Ma) (cf. Ji et al., 2009b). The pre-Cretaceous rocks occur as small relics of varying size within the Cretaceous–early Tertiary Gangdese batholiths that locally intruded the Jurassic–Cretaceous volcano-sedimentary formations (Ji et al., 2009a, b; Mo et al., 2005a; Quidelleur et al., 1997; Wen et al., 2008; Zhang et al., 2007a, 2010a; Zhu et al., 2008b). The pre- and post-Cretaceous suites are lithologically indistinguishable in the field. The widespread and volumetrically significant Tertiary granitoids are characterized by abundant mafic enclaves of the same/similar age (e.g., 50 ± 3 Ma; Mo et al., 2005b).

The central Lhasa subterrane is covered with the widespread Permo-Carboniferous metasedimentary rocks and Late Jurassic–Early Cretaceous volcano-sedimentary rocks, plus minor Ordovician, Silurian, and Triassic limestone (cf. Pan et al., 2004; Zhu et al., 2010 and references therein). The Mesozoic volcanic rocks in this subterrane are mainly Early Cretaceous in age, occurring within the Zenong Group volcano–sedimentary sequence that covers an area of ~2.0×10^4 km^2 from Nam Tso in the east to Gar to the west (Fig. 1b) with an average thickness of up to 1000 m (Zhu et al., 2006). These rocks are predominantly silicic lavas and volcaniclastic rocks with minor andesites and rare basalts (Zhu et al., 2006). Recent zircon U–Pb age results suggest that these rocks were emplaced between 143 and 102 Ma (cf. Zhu et al., 2009b). The Mesozoic plutonic rocks in this subterrane occur as batholiths of varying size, intrude the pre-Ordovician, Carboniferous–Permian metasedimentary successions and Lower Cretaceous volcano-sedimentary succession, and extend discretely for ~1500 km along strike of the subterrane (Fig. 1b). These plutonic rocks have previously been dated to be 215–95 Ma by whole-rock K–Ar and zircon U–Pb methods (He et al., 2006; Zhu et al., 2008a). An important feature of this subterrane is the abundant dioritic enclaves within the Early Cretaceous granitoids (cf. Zhu et al., 2009b).

The sedimentary cover in the northern Lhasa subterrane is mainly Jurassic–Cretaceous with minor Triassic in age (cf. Pan et al., 2004). Voluminous Mesozoic volcanic rocks in this subterrane are exposed within the Lower Cretaceous volcano–sedimentary sequence that extends ~1200 km from Rutong (E80°) to Nagqu (E92°) (Fig. 1b). These rocks consist of andesite, dacite, rhyolite, and associated volcaniclastic rocks. Existing radiometric age data, obtained by Ar–Ar and zircon U–Pb methods (Kapp et al., 2005, 2007; Zhu et al., 2009b), indicate that these rocks were emplaced between ca. 124 and 107 Ma. The Mesozoic plutonic rocks are mainly confined to the western and eastern parts of this subterrane and occur generally as huge batholiths intruding the Jurassic–Lower Cretaceous sedimentary sequences (e.g., Aweng Tso–Yanhu batholiths in the west, Baingoin–Sangba batholiths in the east) (Fig. 1b). These plutonic rocks have previously been dated to be 130–80 Ma mainly by K–Ar, Ar–Ar, and zircon U–Pb methods in the east (Harris et al., 1990; Xu et al., 1985) and ~80 Ma in the west (Zhao et al., 2008). The striking exception is the undeformed Amdo granitoids (Fig. 1b), which intruded the Amdo basement and were previously considered to be emplaced at ~140–120 Ma (Xu et al., 1985), but recent zircon U–Pb dating gives an emplacement age of 185–170 Ma (Guynn et al., 2006).

To obtain a comprehensive dataset of bulk-rock geochemical and zircon isotope data on the Mesozoic–early Tertiary magmatic rocks in the Lhasa Terrane, we collected a total of 400 samples along the Yanhu-Hor, Coqen–Saga, Xainza–Xigaze, and Nyainrong–Nang traverses with a spatial coverage of ~1100 km × 300 km (from E82° to E93° and from N29° to N32°) across the Lhasa Terrane (Fig. 1b). These samples have been analyzed for bulk-rock major and trace element compositions; and 120 of the samples have been selected for *in situ* zircon U–Pb and Hf isotope analysis. Analytical procedures are detailed elsewhere (Hu et al., 2008; Liu et al., 2008, 2010; Wu et al., 2006) and are given in the online supplementary material.

3. Bulk-rock geochemical and zircon isotope data

Bulk-rock major and trace element compositions of 53 samples representative of main rock types with adequate spatial coverage (i.e., along the four traverses across the Lhasa Terrane; Fig. 1b) selected from the 120 samples are given in supplementary Table S1. The zircon isotope data (including a total of 992 U–Pb and 836 Lu–Hf isotopic analyses) for the 53 samples are given in supplementary Tables S2–S3. Cathodoluminescence images of representative zircons and concordia plots are shown in supplementary Fig. S1. Sample details (including GPS position, brief petrography, bulk-rock compositional data, zircon U–Pb isotopic and Hf isotopic data) are summarized in Table 1. Of the 992 U–Pb analyses, 99% have Th/U ratios > 0.1 (Fig. S1; Table S2), consistent with their being of magmatic origin (Hoskin and Schaltegger, 2003). Thus, the interpretation of the zircon U–Pb isotopic data is straightforward and the obtained youngest age group is interpreted as representing the timing of the host rock emplacement. Considering the magmatic phases revealed by recently published age data (cf. Chung et al., 2009; Guynn et al., 2006; Ji et al., 2009a; Lee et al., 2009; Mo et al., 2007, 2008; Wen et al., 2008; Zhang et al., 2010a; Zhou et al., 2008; Zhu et al., 2008b, 2009b, c), the 53 samples reported here are divided into six groups. The bulk-rock compositional and zircon isotope data for each group are shown in Figs. 2–3, and briefly described below. Details for each group are given in online supplementary Appendix A.

3.1. Late Triassic–Early Jurassic (210–175 Ma)

The Late Triassic–Early Jurassic magmatic rocks in the Lhasa Terrane include a variety of rock types with a wide compositional spectrum (60–82 wt.% SiO_2; Fig. 2a). High-K calc-alkalic and shoshonitic series are predominant, but medium-K calc-alkalic rocks are also present (Fig. 2b). In term of aluminum saturation (A/CNK = molar $Al_2O_3/CaO + Na_2O + K_2O$), they are metaluminous to peraluminous (0.87–1.23) (Fig. 2c). Samples dated in this study (Table 1) and granitoids dated in the literature indicate that they were emplaced at 205–178 Ma in the southern Lhasa subterrane (Chu et al., 2006; Ji et al., 2009a; Yang et al., 2008; Zhang et al., 2007a), 210–183 Ma in the central Lhasa subterrane (Liu et al., 2006; Zhang et al., 2007b), and 186–175 Ma in the Nyainrong–Amdo region (Guynn et al., 2006) (Fig. 1b).

Zircons from the Late Triassic samples in the southern Lhasa subterrane display small negative to large positive $\varepsilon_{Hf}(t)$ (−5.0 to +16.2), which contrast the central Lhasa subterrane where the contemporaneous samples exhibit exclusively negative $\varepsilon_{Hf}(t)$ (−17.3 to −2.5) (Fig. 3; Table 1). Zircons from the Early Jurassic samples are dominated by positive $\varepsilon_{Hf}(t)$ (−4.7 to +16.7) in the southern Lhasa subterrane and by negative $\varepsilon_{Hf}(t)$ (−22.0 to +2.0) in the central Lhasa subterrane, respectively (Fig. 3; Table 1). The Late Triassic–Early Jurassic samples from or near the central Lhasa subterrane contain abundant inherited zircons with varying ages (from 2877 to 465 Ma) and $\varepsilon_{Hf}(t)$ (from −18.5 to +9.6) (Fig. 3; Tables S2–S3). The Early Jurassic samples from Nyainrong show exclusively negative $\varepsilon_{Hf}(t)$ (−11.1 to −3.6) (Fig. 3; Table 1).

3.2. Late Jurassic (160–145 Ma)

The Late Jurassic magmatic rocks in the central Lhasa subterrane are silicic (63–76 wt.% SiO_2), high-K calc-alkalic to shoshonitic, and metaluminous to peraluminous (A/CNK = 0.89–1.43) (Fig. 2). Four samples from this subterrane were dated to be 160–146 Ma (Fig. 1b) and exhibit predominantly negative zircon $\varepsilon_{Hf}(t)$ (−16.7 to +1.4) (Fig. 3; Table 1), differing from the contemporaneous granitoids (156–152 Ma) that exhibit $\varepsilon_{Hf}(t) > 0$ in the southern Lhasa subterrane (Ji et al., 2009a).

3.3. Early Cretaceous I (145–118 Ma)

Magmatic rocks of very Early Cretaceous age were identified both in the central and northern Lhasa subterranes. The rocks in the central Lhasa subterrane are silicic (64–78 wt.% SiO_2), medium- to high-K calc-alkalic, and metaluminous to peraluminous (Fig. 2). Five samples from different sites of the central Lhasa subterrane yield U–Pb ages of 143–123 Ma (Fig. 1b) and display exclusively negative zircon $\varepsilon_{Hf}(t)$ (−20.6 to −1.6). By contrast, the rocks of 131–118 Ma in the

Table 1
Summary of bulk-rock geochemical data, zircon U–Pb isotopic ages and Hf isotopic compositions of the Mesozoic–early Tertiary magmatic rocks sampled along the four north–south traverses across the Lhasa Terrane.

No.[a]	Sample		GPS position	Rock type	Mineral assemblage[b]	MME[c]	SiO_2 (wt.%)	A/CNK[d]	Age[e] (Ma)	Zircon ε_{Hf} (t)[f]	Ref.[g]
Late Triassic–Early Jurassic											
1.	NR	NR04-1	N32°06.510′, E92°17.493′	Granodiorite	Pl (50%) + Kfs (15%) + Q (25%) + Bi (8%)	++	71.90	1.05	185.7 ± 1.1	− 5.9 to − 3.6	[1]
2.	NR	NR13-3	N32°04.122′, E92°12.816′	Granodiorite	Pl (40%) + Kfs (30%) + Q (20%) + Bi (8%)	++	64.07	1.06	174.9 ± 1.3	− 10.3 to − 4.1	[1]
3.	NR	NR15-1	N32°00.683′, E92°11.424′	Granodiorite	Pl (40%) + Kfs (30%) + Q (18%) + Bi (10%)	+	69.54	0.95	184.5 ± 1.3	− 11.1 to − 6.2	[1]
4.	NR	08DX17	N30°45.362′, E91°34.967′	Monzogranite	Pl (35%) + Kfs (40%) + Q (18%) + Bi (5%)	−	69.85	1.21	193.6 ± 0.8	− 20.5 to − 16.0	[1]
5.	CL	NML05-1	N30°05.080′, E89°07.000′	Two-mica granite	Kfs (35%) + Pl (15%) + Q (25%) + Bi (15%) + Mus (8%)	−	73.17	1.23	206.0 ± 0.9	− 17.3 to − 3.7	[1]
6.	CL	NML06-1	N30°06.540′, E89°09.460′	Two-mica granite	Kfs (35%) + Pl (20%) + Q (20%) + Bi (10%) + Mus (12%)	−	74.58	1.22	206.5 ± 2.8	− 4.2 to − 2.5	[1]
7.	CL	MB09-1	N30°06.043′, E92°13.768′	Granodiorite	Pl (50%) + Kfs (20%) + Q (20%) + Bi (5%)	++	66.84	0.97	210.2 ± 1.8	− 17.1 to − 6.4	[1]
8.	CL	MB22-1	N29°59.083′, E91°54.358′	Syenogranite	Pl (10%) + Kfs (55%) + Q (25%) + Bi (5%)	++	77.00	1.19	194.9 ± 1.1	(− 22.0) −2.9 to + 1.5	[1]
9.	CL	JD12-1	N30°01.247′, E92°57.690′	Granodiorite	Pl (45%) + Kfs (15%) + Q (25%) + Bi (10%)	+	69.21	0.99	193.2 ± 1.3	− 4.7 to − 3.2	[1]
10.	CL	JD08-1	N29°59.940′, E93°04.652′	Monzogranite	Pl (30%) + Kfs (40%) + Q (20%) + Bi (8%)	+	73.52	1.04	182.9 ± 1.1	− 1.2 to + 2.0	[1]
11.	SL	ML45-1	N29°40.940′, E93°18.733′	Granodiorite	Pl (50%) + Kfs (20%) + Q (20%) + Bi (8%)	+	66.46	0.97	201.3 ± 1.2	− 5.0 to − 3.5	[1]
12.	SL	ML38-5	N29°37.467′, E93°18.417′	Syenogranite	Pl (10%) + Kfs (65%) + Q (20%) + Bi (3%)	+	74.73	1.08	203.2 ± 1.3	− 4.9 to + 2.7	[1]
13.	SL	ML31-1	N29°36.368′, E93°19.277′	Monzogranite	Pl (40%) + Kfs (35%) + Q (25%) + Bi (5%)		74.26	1.03	191.9 ± 1.3	(− 4.7) + 4.9 to + 8.3	[1]
14.	SL	ST134A*	N29°31.200′, E89°37.200′	Granodiorite			72.37	1.13	188.1 ± 1.4	+ 10.0 to + 16.2	[2]
15.	SL	06FW165	N29°30.200′, E89°37.870′	Granodiorite					194.0 ± 3.5	+ 13.4 to + 15.8	[3]
16.	SL	06FW166	N29°30.200′, E89°37.870′	Monzogranite					205.3 ± 3.0	+ 11.9 to + 15.8	[3]
Late Jurassic											
1.	CL	08YR07	N31°48.182′, E82°08.403′	Rhyolite	Q (20%)		75.99	1.43	146.1 ± 0.8	− 10.9 to − 8.5	[1]
2.	CL	08YR09	N31°47.398′, E82°08.426′	Dacite	Pl (15%) + Bi (10%)		66.67	0.98	159.8 ± 0.7	− 16.7 to − 14.1	[1]
3.	CL	MD01-1	N30°38.753′, E85°07.825′	Syenogranite	Kfs (35%) + Pl (20%) + Q (35%) + Bi (8%)	−	74.02	1.12	152.9 ± 1.1	− 4.9 to + 1.4	[1]
4.	CL	MB01-1	N30°09.218′, E92°19.407′	Tonalite	Pl (60%) + Kfs (5%) + Q (20%) + Bi (8%) + Amp (5%)	−	62.83	0.89	154.0 ± 0.8	− 14.2 to − 11.6	[1]
Early Cretaceous I											
1.	NL	YH06-3	N32°17.970′, E82°33.165′	Andesite	Pl (20%) + Bi (5%) + Cpx (5%)		55.52	0.78	131.2 ± 1.4	+ 12.3 to + 18.8	[1]
2.	NL	SB01-2	N30°59.600′, E92°33.340′	Monzogranite	Pl (40%) + Kfs (35%) + Q (20%) + Bi (3%)	−	71.65	1.11	118.4 ± 0.5	− 6.0 to + 5.7	[1]
3.	CL	GJ0611	N32°02.420′, E82°12.040′	Rhyolite			74.39	1.08	143 ± 2	− 11.5 to − 4.9	[4]
4.	CL	GJ0612	N32°02.420′, E82°12.040′	Rhyolite			77.91	1.19	129 ± 1	−7.7 to − 5.2	[4]
5.	CL	08YR11	N31°43.812′, E82°09.182′	Tonalite	Pl (60%) + Kfs (5%) + Q (15%) + Amp (12%) + Bi (5%)	+	63.59	0.93	134.3 ± 1.7	− 9.9 to − 7.7	[1]
6.	CL	08YR14	N31°41.533′, E82°09.996′	Rhyolitic breccia	Q (10%) + Pl (5%)				133.8 ± 1.1	− 11.5 to − 4.3	[1]
7.	CL	08YR16	N31°40.816′, E82°10.550′	Rhyolite	Pl (10%) + Q (5%)		73.35	1.19	142.9 ± 1.0	− 7.1 to − 1.6	[1]
8.	CL	08CQ35	N30°56.343′, E84°34.281′	Monzogranite	Pl (30%) + Kfs (40%) + Q (20%) + Bi (8%)	+	74.33	1.05	122.6 ± 0.8	− 13.8 to − 12.6	[1]
9.	CL	DX13-1	N31°30.080′, E85°10.720′	Dacite	Pl (15%) + Kfs (5%) + Q (10%) + Bi (3%)		68.05	1.04	121 ± 1	− 10.2 to − 6.6	[4]
10.	CL	DX2-1	N31°27.510′, E84°56.080′	Dacite	Pl (20%) + Kfs (5%) + Q (5%) + Bi (5%)		66.48	1.03	130 ± 1	− 10.7 to − 5.2	[4]
11.	CL	MB05-7	N30°06.067′, E92°19.557′	Monzogranite	Pl (35%) + Kfs (40%) + Q (20%) + Bi (3%)	+	71.64	1.06	129.9 ± 1.0	(− 20.6) −7.0 to − 5.6	[1]
12.	SL	MM02-3	N29°15.210′, E91°58.530′	Adakitic andesite	Pl (15%) + Amp (5%)		54.88	0.90	136.5 ± 1.7	+ 10.6 to + 12.4	[5]
Early Cretaceous II											
1.	NR	NR18-1	N31°56.751′, E92°09.328′	Granodiorite porphyry	Pl (15%) + Bi (10%) + Q (5%)		66.40	0.95	110.4 ± 0.7	− 3.5 to + 0.6	[1]
2.	NR	NQ16-1	N31°47.360′, E92°04.097′	Monzogranite			71.64	1.05	117.5 ± 0.7	− 10.2 to − 5.0	[1]
3.	NL	YH15-1	N32°30.058′, E82°26.722′	Monzogranite	Pl (35%) + Kfs (40%) + Q (15%) + Bi (8%)	−			110.1 ± 0.7	+ 5.0 to + 8.9	[1]
4.	NL	YH22-4	N32°21.175′, E82°26.862′	Rhyolite	Pl (15%) + Kfs (10%) + Q (5%) + Bi (5%)		75.54	1.03	110.6 ± 0.6	+ 4.7 to + 9.2	[1]

5.	NL	YH04-2	N32°17.084′, E82°32.858′	Andesite	Pl (30%)		55.61	0.81	116.7 ± 1.2	+ 13.5 to + 18.4	[1]
6.	NL	YH01-2	N32°16.318′, E82°31.392′	Rhyolite	Pl (10%) + Q (15%)		73.98	1.15	109.0 ± 1.0	+ 6.8 to + 11.9	[1]
7.	NL	NM01-1	N31°50.630′, E87°05.250′	Dacite	Pl (25%)		62.88	1.02	111.9 ± 0.9	+ 7.7 to + 10.1	[1]
8.	NL	DG05-1	N31°19.700′, E88°54.890′	Dacite	Pl (25%) + Bi (5%) + Q (3%)		67.06	1.04	114.3 ± 0.6	− 0.9 to + 1.9	[1]
9.	NL	DG01-1*	N31°21.270′, E88°55.800′	Rhyolite	Kfs (20%) + Pl (15%) + Q (3%)		74.36	1.20	115.7 ± 0.6	− 1.5 to + 4.2	[6]
10.	NL	NQ12-10	N31°28.803′, E92°06.433′	Andesite	Pl (20%) + Bi (10%)		59.51	0.90	110.8 ± 0.6	− 10.0 to − 7.7	[1]
11.	NL	NQ09-1	N31°45.971′, E92°37.403′	Monzogranite	Pl (40%) + Kfs (35%) + Q (15%) + Bi (8%)		69.29	0.98	110.7 ± 0.8	− 6.8 to + 0.9	[1]
12.	NL	08DX21	N31°02.859′, E91°41.445′	Syenogranite	Pl (20%) + Kfs (50%) + Q (20%) + Bi (8%)		75.64	1.07	110.7 ± 0.6	− 5.8 to − 4.5	[1]
13.	CL	DXL1-3	N31°39.310′, E85°11.700′	Rhyolitic tuff			73.95	0.90	112 ± 1	− 0.6 to + 2.9	[4]
14.	CL	DX19-1	N31°16.910′, E85°07.570′	Granodiorite	Pl (50%) + Q (25%) + Kfs (10%) + Bi (8%) + Amp (3%)		71.10	1.01	107 ± 1	− 1.4 to + 2.6	[4]
15.	CL	DX21-1	N31°00.000′, E85°07.020′	Rhyolite	Q (25%) + Pl (12%) + Kfs (8%)		75.30	1.16	111 ± 1	− 5.8 to − 0.2	[4]
16.	CL	NX5-2	N30°45.660′, E85°31.850′	Granodiorite	Pl (45%) + Kfs (28%) + Q (20%) + Amp (5%)	++	67.52	1.00	109 ± 1	− 6.7 to − 2.6	[4]
17.	CL	NX5-3	N30°45.660′, E85°31.850′	Diorite	Pl (50%) + Q (20%) + Amp (18%) + Bi (10%)		57.41	0.82	108 ± 1	− 7.2 to − 0.7	[4]
18.	CL	GB-8	N30°45.560′, E85°32.250′	Granodiorite	Pl (40%) + Kfs (30%) + Q (20%) + Bi (5%)	+	68.43	0.95	116 ± 1	− 7.5 to − 3.5	[4]
19.	CL	GRC02-1	N31°03.980′, E88°12.410′	Dacite	Pl (30%) + Q (10%) + Bi (3%)		64.61	1.13	114.0 ± 0.7	− 14.4 to − 4.1	[1]
20.	CL	GRC03-2	N31°13.570′, E88°07.610′	Dacite	Pl (25%) + Q (10%)		65.28	1.03	113.8 ± 0.5	− 11.8 to − 4.5	[1]
21.	CL	SZ10-1	N30°53.400′, E88°39.740′	Dacite	Q (25%) + Pl (20%) + Bi (10%)		64.45	1.35	112.1 ± 0.4	− 7.8 to − 4.7	[1]
22.	CL	SZ01-1*	N30°45.380′, E88°55.340′	Dacite	Pl (30%) + Q (20%) + Bi (5%)		64.81	0.82	116.7 ± 0.6	− 8.6 to − 4.7	[6]
23.	CL	SZ07-1	N30°45.960′, E88°54.080′	Dacite	Pl (20%) + Bi (15%)		63.51	1.04	110.9 ± 0.5	− 9.0 to − 4.6	[1]
24.	SL	06FW170	N29°23.570′, E89°37.700′	Diorite					108.6 ± 1.5	+ 11.2 to + 13.9	[3]
Late Cretaceous											
1.	NL	ZGP06-1*	N31°32.290′, E87°29.970′	Dacite	Pl (40%) + Cpx (10%)		65.77	1.02	91.0 ± 0.8	+ 5.2 to + 8.2	[7]
2.	CL	MB12-1	N30°04.515′, E92°09.248′	Granodiorite	Pl (50%) + Kfs (20%) + Q (25%) + Bi (3%)	−	68.48	0.90	88.3 ± 0.5	− 3.8 to − 1.7	[8]
3.	SL	08YR27	N31°03.615′, E82°11.630′	Rhyolite	Q (20%) + Pl (5%)		78.19	1.32	80.6 ± 0.6	− 4.0 to + 0.5	[1]
4.	SL	RGZ01-1	N29°15.920′, E90°24.700′	Diorite	Pl (60%) + Q (15%) + Bi (15%) + Cpx (8%)		56.96	0.91	87.4 ± 1.0	+ 12.0 to + 14.9	[1]
5.	SL	NML01-1	N29°26.450′, E89°05.670′	Diorite	Pl (60%) + Q (10%) + Kfs (5%) + Bi (12%) + Amp (8%) + Cpx (3%)		57.46	0.85	87.7 ± 1.2	+ 10.8 to + 12.8	[1]
6.	SL	ML11-1	N29°06.792′, E93°27.117′	Monzogranite	Pl (30%) + Kfs (40%) + Q (25%) + Bi (3%)	−			82.2 ± 0.7	+ 10.2 to + 14.5	[1]
7.	SL	ML06-1	N29°03.433′, E93°22.813′	Granodiorite	Pl (45%) + Kfs (20%) + Q (20%) + Bi (10%) + Cpx (3%)	−	70.58	1.00	79.3 ± 0.4	+ 10.4 to + 12.3	[1]
8.	SL	ML01-1	N29°00.365′, E93°18.907′	Tonalite	Pl (55%) + Kfs (5%) + Q (25%) + Bi (10%) + Amp (3%)	−	66.19	0.95	84.2 ± 1.1	+ 9.6 to + 14.6	[1]
Early Tertiary											
1.	SL	08YR28	N31°00.524′, E82°09.565′	Andesite	Pl (20%) + Kfs (5%) + Q (5%)		59.81	0.84	50.8 ± 0.4	− 1.9 to − 0.2	[1]
2.	SL	08YR29	N30°58.128′, E82°10.980′	Dacite	Pl (10%) + Q (5%)				61.2 ± 1.5	− 1.6 to + 0.4	[1]
3.	SL	08YR30	N30°53.926′, E82°09.145′	Monzogranite		−	72.94	1.01	54.2 ± 0.5	+ 7.2 to + 10.5	[1]
4.	SL	08CQ13	N30°08.213′, E85°24.528′	Diorite	Pl (60%) + Kfs (10%) + Q (5%) + Bi (15%) + Amp (8%)		54.04	0.81	51.5 ± 0.4	− 2.4 to 2.6	[1]
5.	SL	08CQ09	N29°53.717′, E85°44.454′	Granodiorite porphyry	Pl (15%) + Bi (10%)	++	68.52	0.96	50.0 ± 0.4	− 2.2 to + 3.0	[1]
6.	SL	08CQ03	N29°46.881′, E85°45.484′	Monzogranite	Pl (35%) + Kfs (30%) + Q (20%) + Bi (10%) + Amp (3%)	++	67.92	0.95	51.9 ± 0.4	− 2.1 to + 3.5	[1]
7.	SL	08CQ02	N29°37.504′, E85°44.605′	Syenogranite	Pl (15%) + Kfs (60%) + Q (20%) + Bi (3%)	−	78.07	1.06	43.9 ± 0.3	− 2.0 to + 4.2	[1]
8.	SL	NML03-1	N29°37.348′, E89°03.641′	Diorite	Pl (50%) + Q (10%) + Amp (25%) + Bi (18%)		58.03	0.92	62.4 ± 0.3	+ 5.5 to + 7.2	[1]

[a] NR = Nyainrong, NL = Northern Lhasa subterrane, CL = Central Lhasa subterrane, SL = Southern Lhasa subterrane.
[b] Pl = plagioclase; Kfs = K-feldspar; Amp = amphibole; Cpx = clinopyroxene; Bi = biotite; Mus = Muscovite. Only phenocryst minerals are listed for volcanic rocks and porphyries.
[c] "+ +" = abundant, "+" = occurred, "−" = rare or absent.
[d] A/CNK = molecular $Al_2O_3/(CaO + Na_2O + K_2O)$.
[e] *Dated by SHRIMP with 1σ uncertainty; others are dated by LA-ICPMS with 2σ uncertainty.
[f] Data in bracket are "outlier" zircon grains.
[g] [1] = this study; [2] = Chu et al. (2006); [3] = Ji et al. (2009a); [4] = Zhu et al. (2009b); [5] = Zhu et al. (2009c); [6] = Zhu et al. (submitted for publication-a); [7] = Wang et al. (unpublished); [8] = Meng et al. (2010).

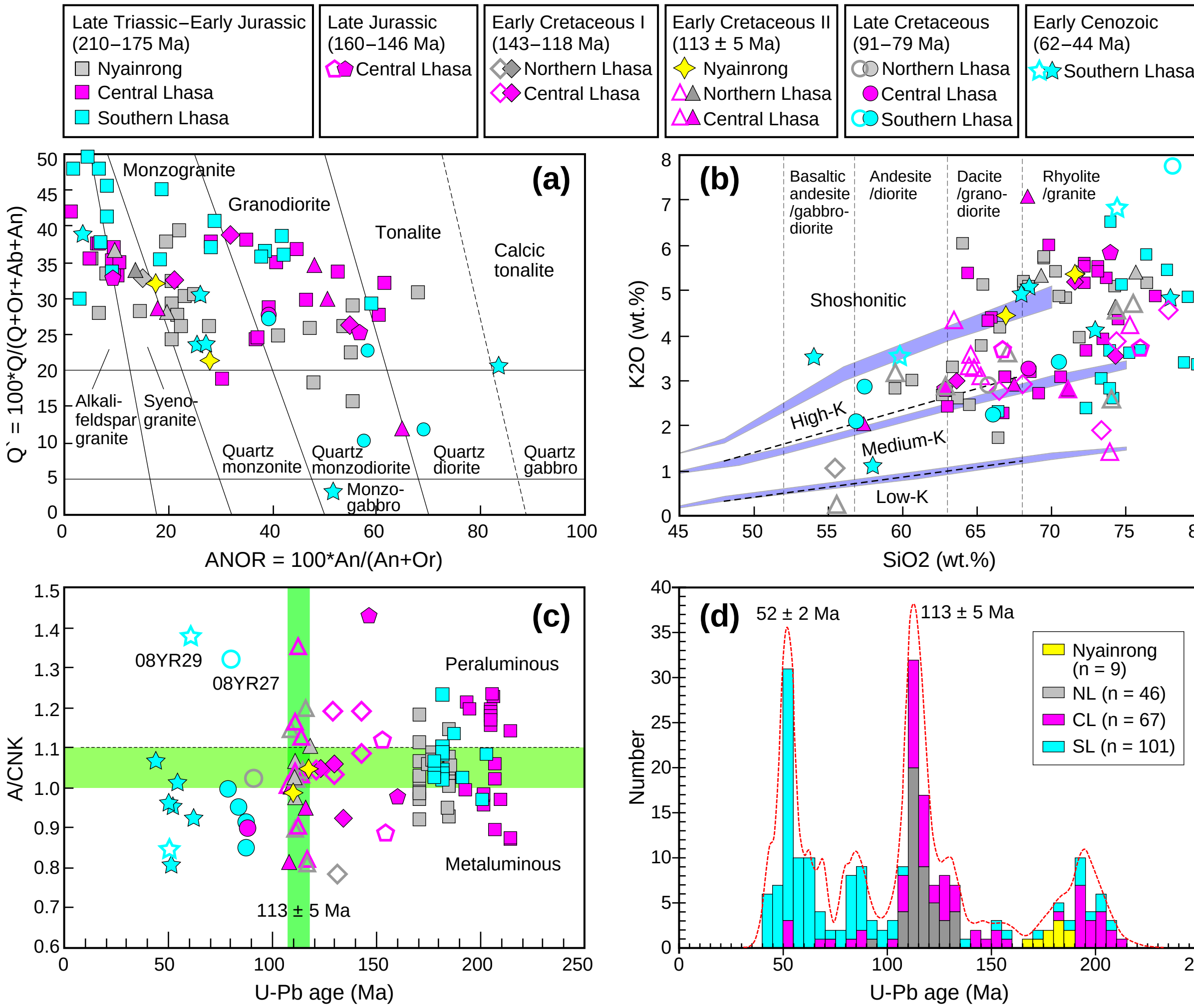

Fig. 2. (a) Normative classification of granitoid rocks (Streckeisen and Le Maitre, 1979); (b) SiO_2–K_2O (Peccerillo and Taylor1976) showing sample compositional variation; (c) Plot of aluminum saturation index [i.e. A/CNK = molecular $Al_2O_3/(CaO + Na_2O + K_2O)$] vs. U–Pb age of the Mesozoic–early Tertiary magmatic rocks in the Lhasa Terrane (Yang et al., 2008; this study; our unpublished data); (d) Histogram of age dates for the Mesozoic–early Tertiary magmatic rocks in the Lhasa Terrane (Ji et al., 2009a; Zhu et al., 2009a, b; this study; our unpublished data; Zhang et al., 2010a). The filled and unfilled symbols represent granitoids and volcanic rocks, respectively.

northern Lhasa subterrane (Fig. 1b) are more mafic (56–72 wt.% SiO_2), medium-K calc-alkalic to shoshonitic, metaluminous to peraluminous (Fig. 2), and are dominated by positive zircons $\varepsilon_{Hf}(t)$ (−6.0 to +18.8) (Fig. 3; Table 1).

3.4. Early Cretaceous II (113 ± 5 Ma)

Magmatic rocks of late Early Cretaceous age are widespread in the central and northern Lhasa subterranes, while the contemporaneous rocks from the Gangdese batholiths in the southern Lhasa subterrane may have been eroded owing to orogenic uplift and erosion (Wu et al., 2010). The rocks from the central Lhasa subterrane are mostly silicic (57 to 75 wt.% SiO_2) and high-K calc-alkalic. They are metaluminous to peraluminous (A/CNK = 0.82–1.35) (Fig. 2). Four samples from Xainza in this subterrane were dated to be 114–111 Ma (Fig. 1b) and exhibit exclusively negative zircon $\varepsilon_{Hf}(t)$ (−14.4 to −4.1) (Fig. 3; Table 1). No inherited zircons older than 140 Ma are present in these samples (Table S2).

The rocks in the northern Lhasa subterrane span a wide compositional spectrum (56–76 wt.% SiO_2) (Fig. 2a). High-K calc-alkalic series are dominant, but low- to medium-K calc-alkalic varieties are also present (Fig. 2b). They are metaluminous to peraluminous (A/CNK = 0.81–1.20) (Fig. 2c). Eleven samples including a variety of rock types give zircon crystallization ages of 118–109 Ma (Fig. 1b), and exhibit a general decrease in zircon $\varepsilon_{Hf}(t)$ from west (+4.7 to +18.4) via central (−1.5 to +10.1) to east (−10.0 to +0.9) (Fig. 3; Table 1) in this subterrane.

3.5. Late Cretaceous (90–80 Ma)

Late Cretaceous rocks in the southern Lhasa subterrane are dominated by diorite and granodiorite (57–71 wt.% SiO_2) (Fig. 2a) with medium- to high-K calc-alkalic and metaluminous characteristics (A/CNK = 0.85–1.00) (Fig. 2c). Five samples yield U–Pb ages of 88–79 Ma (Fig. 1b) with positive zircon $\varepsilon_{Hf}(t)$ of +9.6 to +14.9, which are identical to those of the coeval granodiorites near Quxu (Ji et al., 2009a). An exception is the occurrence of the strongly peraluminous rhyolite (A/CNK = 1.32) of ~81 Ma from northeast of Hor in the southern Lhasa subterrane (Fig. 1b), which yields $\varepsilon_{Hf}(t)$ (−4.0 to +0.5) similar to the contemporaneous granitoids (−3.8 to −1.7) in the central Lhasa subterrane (Meng et al., 2010; Table 1).

3.6. Early Tertiary (65–44 Ma)

The magmatic rocks of early Tertiary age are limited to the southern Lhasa subterrane. They are compositionally diverse (54–78 wt.% SiO_2), varying from high-K calc-alkalic to shoshonitic, and from metaluminous to peraluminous (A/CNK = 0.81–1.38) (Fig. 2).

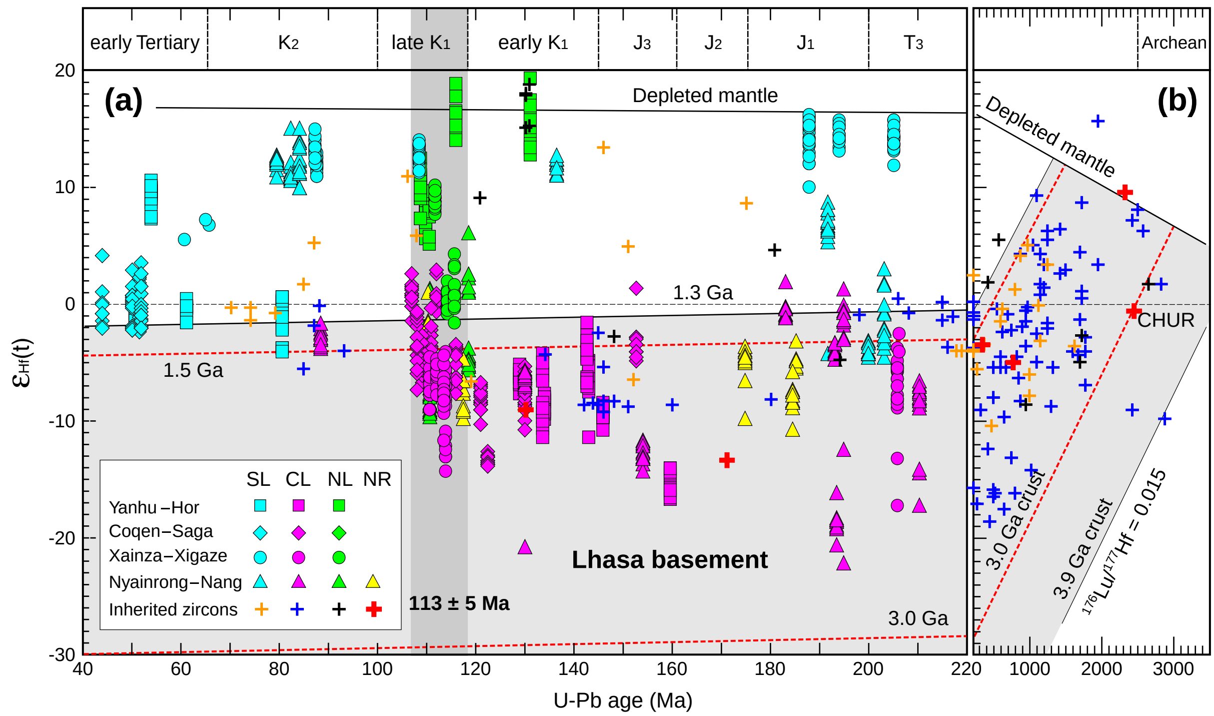

Fig. 3. Plots of $\varepsilon_{Hf}(t)$ (parts per 10^4 deviation of initial Hf isotope ratios between zircon samples and the chondritic reservoir at the time of zircon crystallization) vs. ages of the Mesozoic–early Tertiary magmatic rocks from the four north–south sampling traverses across the Lhasa Terrane. The sub-horizontal lines in Fig. 3 are Hf "crustal" model ages (T^{C}_{DM}), which are calculated by assuming its parental magma to have been derived from an average continental crust (with $^{176}Lu/^{177}Hf = 0.015$) that originated from the depleted mantle source (Griffin et al., 2002). Zircon Hf isotopic compositions indicate the presence of the hidden Precambrian basement as old as Archean age in both the central Lhasa subterrane (shade area, up to 3.9 Ga) and Nyainrong region (red broken line, up to 3.0 Ga). Abbreviations: NR = Nyainrong, others are the same as in Fig. 1. See text for details.

Eight samples from the western part give zircon U–Pb ages of 62–44 Ma (Fig. 1b), coeval with rocks from the eastern part of this subterrane (Ji et al., 2009a; Lee et al., 2009; Mo et al., 2008; Wen et al., 2008). Zircons from these samples exhibit small negative to large positive $\varepsilon_{Hf}(t)$ (−2.4 to +10.5) (Fig. 3; Table 1). A diorite sample from south of Namling (Fig. 1b) contains abundant inherited zircons with a large age range (1632–108 Ma; Table S2), and those of >460 Ma show varying $\varepsilon_{Hf}(t)$ (−10.3 to +4.4), comparable to $\varepsilon_{Hf}(t)$ of inherited zircons from the central Lhasa subterrane (Fig. 3; Table S3).

3.7. Summary

The new zircon U–Pb age data from the four traverses reported here, in combination with the data on magmatic rocks of Mesozoic–early Tertiary age reported in the recent literature from other sites of the Lhasa Terrane (cf. Guynn et al., 2006; Ji et al., 2009a; Wen et al., 2008; Zhang et al., 2010a; Zhu et al., 2009b, c, unpublished data), are illustrated in the form of histogram (Fig. 2d). This, together with the bulk-rock geochemical and zircon Hf isotopic data (Fig. 3) presented above, shows that: (i) the rocks appear to be emplaced continuously from the Late Triassic to Early Tertiary (220–40 Ma) in the Lhasa Terrane; (ii) the rocks were emplaced mostly in two intense episodes with peaks at about 113 and 52 Ma, which geographically correspond to the present-day outcrop areas in the central/northern Lhasa subterranes and southern Lhasa subterrane, respectively; (iii) the rocks emplaced during each of the two episodes are all compositionally diverse, ranging from metaluminous (A/CNK<1.1, corresponding to I-type granite) to peraluminous (A/CNK>1.1, corresponding to S-type granite) varieties; (iv) the northern Lhasa subterrane exposes varying rock types (andesite, dacite, rhyolite, and granitoids) with predominantly positive zircon $\varepsilon_{Hf}(t)$, which contrast the central Lhasa subterrane where silicic rocks are dominated by zircons with $\varepsilon_{Hf}(t) < 0$; and (v) there is significant zircon $\varepsilon_{Hf}(t)$ change from the older rocks to the 113 ± 5 Ma rocks, i.e., in the central Lhasa subterrane the zircon $\varepsilon_{Hf}(t)$ tends to increase with time, while in the northern Lhasa subterrane it tends to decrease.

4. Discussion

4.1. Lithospheric architecture of the Lhasa Terrane

In the vast Lhasa Terrane, the gneissic basement rocks are only found in Amdo and its vicinity (Fig. 1b) (Guynn et al., 2006; Xu et al., 1985). Hence, the spatial extent and nature of the crystalline basement beneath the entire terrane has been speculative and relying on geophysical interpretations (e.g., Kosarev et al., 1999; McKenzie and Priestley, 2008; Tilmann et al., 2003) or interpretations of whole-rock Nd isotope data on clastic sedimentary rocks (Zhang et al., 2007c). Although surface wave tomography records an increase in lithospheric thickness beneath north of ~30°N in the Lhasa Terrane where lithospheric structure similar to that of Archaean and Proterozoic cratons is inferred to exist (McKenzie and Priestley, 2008), the nature and history of the lithospheric mantle and crustal basement remains unknown because seismic tomography provides no age information.

Zircon Hf isotopes offer a powerful tool in this regard (Flowerdew et al., 2009; Griffin et al., 2002; Kemp et al., 2006). Fig. 4 plots Hf isotope data of zircons from the four traverses against latitude of sample locations. Along each of the traverses, zircon $\varepsilon_{Hf}(t)$ values all decrease from the northern and southern subterranes with small negative to large positive $\varepsilon_{Hf}(t)$ values towards the central Lhasa subterrane with large negative to small positive $\varepsilon_{Hf}(t)$ values. It is also important to note (i) that the inherited zircons of Archean age (up to ~2877 Ma with a "crustal" model age as old as 3.85 Ga) and the very large negative $\varepsilon_{Hf}(t)$ values of zircons representing the timing of the host rock emplacement (up to −22.0 with Paleoproterozoic to Archean "crustal" model ages) (e.g., samples 08YR09, 08CQ35, 08DX17, MB05-7, and MB22-1) in the central Lhasa subterrane (Fig. 3; Table S3) actually require the presence of Paleoproterozoic to

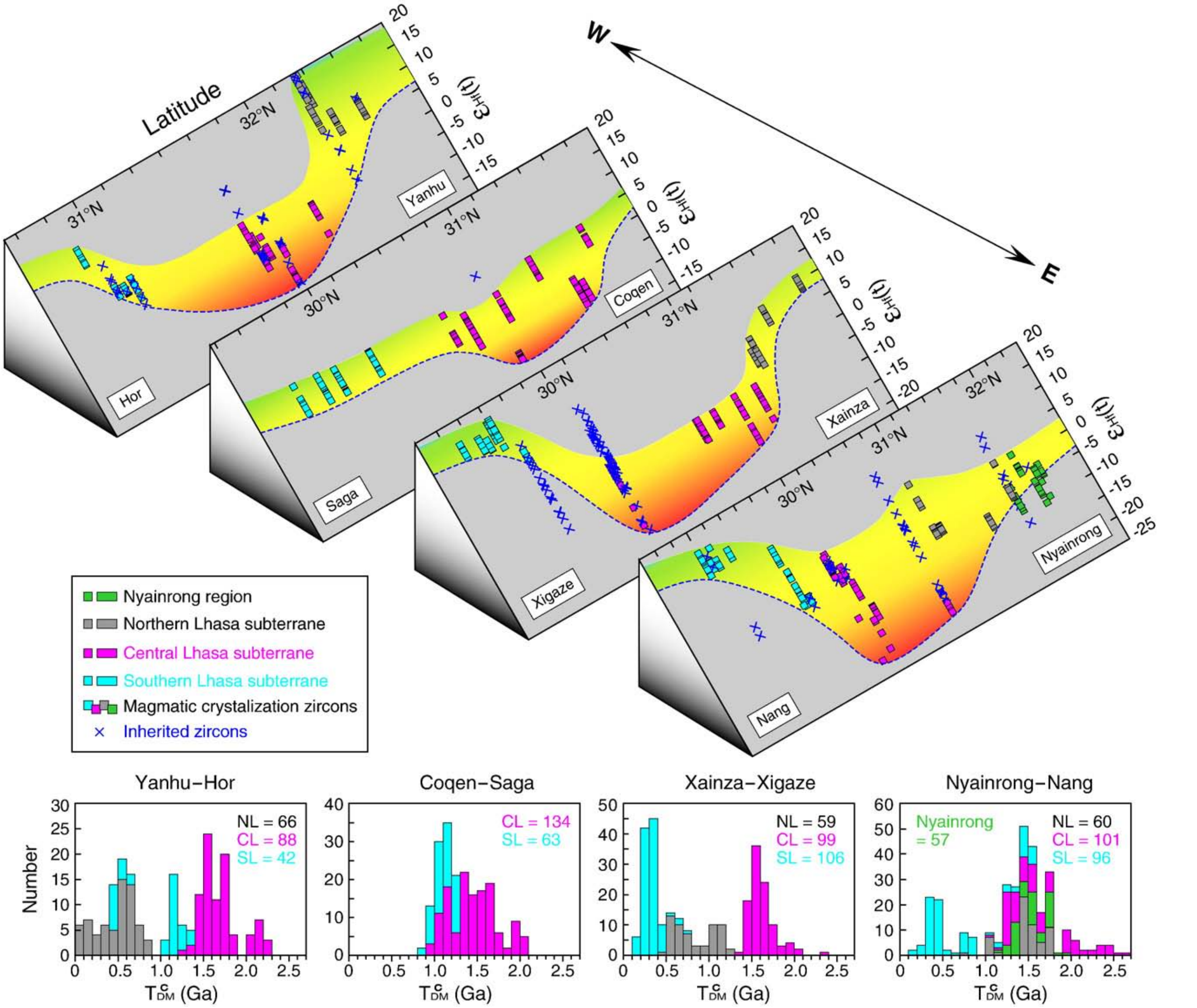

Fig. 4. The range and spatial distribution of $\varepsilon_{Hf}(t)$ values, and the histogram of Hf "crustal" model ages ($T_{DM}{}^C$) of zircons from the Mesozoic–early Tertiary magmatic rocks in the Lhasa Terrane. Zircon $\varepsilon_{Hf}(t)$ values plotted against sample latitude, showing to a first-order consistent profiles indicating the presence of ancient crustal materials in the central Lhasa subterrane and juvenile crustal materials in the northern and southern accreted subterranes. The color bands indicate the ranges of $\varepsilon_{Hf}(t)$ values of zircons at the time (t) of crystallization. The histograms of Hf "crustal" model ages ($T_{DM}{}^C$) using individual analyses indicate the presence of an older "hidden crust" beneath the central Lhasa subterrane (Mesoproterozoic to Archean) than the northern (Phanerozoic to Mesoproterozoic) and southern (Phanerozoic) Lhasa subterranes and of a Meso- to Paleoproterozoic "hidden crust" beneath the Nyainrong region. Abbreviations are the same as in Fig. 1.

Achaean basement although it has not been directly sampled, and (ii) that the dominantly positive $\varepsilon_{Hf}(t)$ values (-1.9 to $+8.3$ with an average of $+3.9$) in zircons of the 134–125 Ma granitoids from the Baingoin batholith (Fig. 1b) (Zhu et al., submitted for publication-a) resemble $\varepsilon_{Hf}(t)$ values in zircons of granitoid rocks west of the Baingoin in the northern Lhasa subterrane, all indicating the presence of a juvenile crust and a host magma source in the mafic lower crust derived from the mantle in no distant past.

Because crust–mantle interaction is inevitable during mantle melting (e.g., melting of subducted sediments) and melt emplacement (e.g., crustal assimilation), the measured $\varepsilon_{Hf}(t)$ values represent mixing between the mantle (i.e., large $+\ \varepsilon_{Hf}(t)$) and mature crust (large $-\ \varepsilon_{Hf}(t)$) end-members. Hence, the positive $\varepsilon_{Hf}(t)$ for the juvenile crust in the northern and southern subterranes is likely underestimated, and should be more positive and the "crustal" model age should be even younger, which can result from juvenile crust-derived melts that have mixed with varying contributions from anatexis of ancient crustal materials or subducted terrigeneous sediments. Conversely, the negative $\varepsilon_{Hf}(t)$ for the reworked crust toward the central Lhasa subterrane is likely overestimated, and should be more negative and the "crustal" model age should be even older, which can be accounted for by mixing between melts largely derived from anatexis of ancient continental crustal materials and minor basalt-derived melts. Therefore, the profiles of zircon $\varepsilon_{Hf}(t)$ distribution with latitude in Fig. 4 should be more extreme, i.e., even more negative $\varepsilon_{Hf}(t)$ (more ancient than Paleoproterozoic) in the central Lhasa subterrane, and even more positive $\varepsilon_{Hf}(t)$ (more juvenile and younger than Mesoproterozoic) in the southern and northern Lhasa subterranes. This finding offers smoking-gun evidence for the presence of Paleoproterozoic and Archean basement (up to 2877 Ma) beneath the central Lhasa subterrane. It follows that the central Lhasa subterrane once must be a microcontinent. This continent had acted as a nucleus to which juvenile crust has been accreted in the northern and southern subterranes in the Phanerozoic during its journey of drift across the Tethyan Ocean basins and ultimate continental collisions.

It is noteworthy that the zircon $\varepsilon_{Hf}(t)$ distinction between the central Lhasa subterrane and the northern and southern subterranes is also reflected in sedimentary cover rocks (see above) and corresponds well to the northern, central and southern subterranes (cf. Zhu et al., 2009a, b, 2010). These subterranes are separated (i) by the Shiquan River–Nam Tso Mélange Zone (SNMZ) (Pan et al., 2004) that may document the evolution of a back-arc basin likely developed in the Early Cretaceous (Baxter et al., 2009; Zhang et al., 2004) and (ii) by the Luobadui–Milashan Fault (LMF) (Pan et al., 2004) that correlates in space with a newly recognized Carboniferous–Permian suture zone (Yang et al., 2009) (Fig. 1b). Furthermore, the transition from the southern Lhasa juvenile crust to central Lhasa mature crust along the LMF coincides well with the present-day change in lithospheric thickness (Fig. 4a of McKenzie and Priestley, 2008), which may suggest that the thick lithosphere beneath the present-day Lhasa Terrane is inherited, at least partly, from its Mesozoic precursor. By contrast, the northern transition from the central Lhasa reworked crust to northern Lhasa juvenile crust along the SNMZ has not been detected by the present-day geophysical methods (e.g., McKenzie and Priestley, 2008), which could be due to crustal shortening and lithosphere thickening in response to the Qiangtang–Lhasa collision and subsequent intracontinental convergence (cf. Kapp et al., 2007).

4.2. Geodynamic setting and tectonomagmatic evolution of the Lhasa Terrane in the Mesozoic

4.2.1. Generation of the Late Triassic–Early Jurassic magmatic rocks

The Late Triassic–Early Jurassic (~205–174 Ma) magmatic rocks in the southern Lhasa subterrane have been interpreted as a result of northward subduction of the Neo-Tethyan Ocean seafloor (Chu et al., 2006; Ji et al., 2009a; Yang et al., 2008; Zhang et al., 2007a; Zhu et al., 2008b) whereas the coeval peraluminous granitoids (~206–190 Ma; ~50 km north of the southern subterrane) in the central Lhasa subterrane are consistent with an origin within a late- to post-collisional setting (Liu et al., 2006; Zhang et al., 2007b). These rocks are only slightly younger than the earliest radiolarian assemblages of Ladinian–Carnian age (237–217 Ma) from chert sequences within the Indus–Yarlung–Zangbo suture (IYZSZ), which likely indicate a rifting marginal basin (Zhu et al., 2005) (evolved to what is known as the Neo-Tethyan Ocean). This means that the southern edge of the central Lhasa subterrane had only just formed as a passive margin rather than a mature active continental margin with a subduction zone. Hence, the above tectonomagmatic interpretation needs revision. Although more work is needed, the current data allow two general statements on the generation of these rocks.

First, the zircon $\varepsilon_{Hf}(t)$ (mostly <0; Fig. 3) data indicate that the Late Triassic–Early Jurassic granitoids from the central Lhasa subterrane and Nyainrong region are dominated by melts derived from ancient, pre-existing, mature continental crust material, giving bulk compositions similar to S-type granitoids. In contrast, the zircon $\varepsilon_{Hf}(t)$ (mostly >0; Fig. 3) data of the contemporaneous granitoids from the southern Lhasa subterrane indicate that the granitoids are isotopically dominated by melts derived from mafic source material of mantle origin with limited contributions from the mature continental crust, giving bulk compositions similar to I-type granitoids and representing net juvenile crust accretion. The latter is best explained by remelting of pre-existing underplated and metasomatised mafic crust resulting from the northward subduction of the Paleo-Tethyan Ocean seafloor represented by the Songdo eclogite during the Late Paleozoic (Yang et al., 2009; Zhu et al., 2009a, 2010) under hydrous amphibolite facies conditions (Niu, 2005).

Second, geochronological data indicate that the Amdo basement experienced amphibolite facies metamorphism at 185–170 Ma (Guynn et al., 2006; Xu et al., 1985) and granulite facies metamorphism at about 169 Ma (Zhang et al., 2010b) that is coeval with the late phase of the Amdo–Nyainrong granitoid magmatism (Guynn et al., 2006; this study). We interpret the late metamorphism and magmatism as resulting from a single event, most likely a collision event related to the Amdo–Qiangtang collision (Guynn et al., 2006) rather than the Lhasa–Qiangtang collision (Xu et al., 1985). This is because paleomagnetic (Li et al., 2004), stratigraphic and paleontological data (Leeder et al., 1988; Metcalfe, 2010; Yin et al., 1988;, and references therein) indicate that a wide ocean was still present between the Lhasa and Qiangtang Terranes during the Early Jurassic.

4.2.2. Southward subduction of the Bangong–Nujiang Ocean seafloor

The northward subduction of the Neo-Tethyan Ocean seafloor beneath the southern Lhasa subterrane has been well established and continued until the India–Asia collision in the Early Cenozoic. However, the subduction direction of the seafloor of the Bangong–Nujiang Ocean north of the Lhasa Terrane has been in debate for sometime (e.g., Allègre et al., 1984; Dewey et al., 1988; Kapp et al., 2007; Xu et al., 1985; Zhang et al., 2004). The presence of low-K to high-K calc-alkaline andesite–dacite–rhyolite suite of 131–110 Ma (Fig. 2b) with positive zircon $\varepsilon_{Hf}(t)$ west of Baingoin (this study) and granitoids of 134–125 Ma with positive zircon $\varepsilon_{Hf}(t)$ from Baingoin batholiths (Zhu et al., submitted for publication-a) in the northern Lhasa subterrane is consistent with southward subduction of the Bangong–Nujiang seafloor beneath the Lhasa Terrane. More importantly, zircon Hf isotopic data of the Mesozoic–early Tertiary rocks from the four north–south traverses (Fig. 1b) clearly reveal an apparent southward (i.e., continentward) decrease in $\varepsilon_{Hf}(t)$ across the northern and central Lhasa subterranes (Fig. 4). Such feature is similar to the variation of bulk-rock $\varepsilon_{Nd}(t)$ in the southern Lhasa subterrane (Zhu et al., 2008b) and other continental margin batholiths (e.g. Sierra Nevada and Peninsular Ranges in California) (DePaolo et al., 2008) where continentward subduction occurred, confirming southward subduction of the Bangong–Nujiang seafloor beneath the northern Lhasa subterrane.

It remains unknown, however, when and how the subduction was initiated at the northern edge of the central Lhasa subterrane. The continental nature of the central Lhasa subterrane lithosphere architecture ascertains that regardless of its actual size, an ancient compositionally depleted and thus physically buoyant lithospheric root is required (i) to maintain its integrity (Abbott et al., 1997; Jordan, 1988; Niu et al., 2003) in the course of its drift in an otherwise vast ocean basin setting (e.g., the Lhasa microcontinent drifting across the Tethys), (ii) to develop subduction zones at its edges (Niu et al., 2003) allowing the dense oceanic lithosphere to subduct towards beneath it, and (iii) to induce subduction/convergence-related magmatism for net crustal growth. These mean that the rift ocean basin (evolved to what is known as the Neo-Tethys south of the Lhasa Terrane) must have a passive margin at the southern edge of the central Lhasa subterrane in its early history, making its northward drift possible. The latter also requires that the ocean basin (known as the Bangong–Nujiang Tethys) north of the northward drifting central Lhasa subterrane shrink by means of seafloor subduction. A subduction zone may be present at the northern rim of the Bangong–Nujiang Tethyan Ocean (e.g., represented by the Jinsha suture zone; Pan et al., 2004), but the progressive decrease in $\varepsilon_{Hf}(t)$ values of zircons from the northern to central Lhasa subterranes (Fig. 4) indicate that a subduction zone may have already existed at the northern edge of the central Lhasa subterrane for some time, perhaps, prior to the separation of the central Lhasa subterrane from Gondwana. Such a southward subduction may have been triggered by the central Lhasa–Australia collision at the end of the Middle Permian (ca. 263 Ma; Zhu et al., 2009a) that led to the closure of the Paleo-Tethyan Ocean Basin south of the central Lhasa subterrane (Yang et al., 2009), and played a critical role in the separation of the central Lhasa subterrane from Gondwana (Australian?) by creating a back-arc basin that would have developed and evolved into the Neo-Tethyan Ocean (Ferrari et al., 2008; Niu et al., 2003; Sengör, 1979;).

It should be pointed out that the above geodynamic consideration requires the presence of a mélange zone (i.e., Permian–Triassic mélange zone) along the northern edge of the Lhasa Terrane. Further work is underway, and several recent studies have indeed indicated its presence: (1) the identification of angular unconformity between the Upper Triassic flysch with basal conglomerate that contains ophiolitic elements and the underlying ophiolites in Baila (Chen et al., 2005; Pan et al., 2006), and (2) the possible existence of the late Paleozoic ophiolites southwest of Nagqu, where the cumulate gabbro has been dated to be ~242 and 259 Ma (Nimaciren et al., 2005).

4.2.3. Tectonomagmatic evolution during the Mesozoic

The Amdo basement located between the present-day Lhasa and Qiangtang Terranes (Fig. 1b) has traditionally been considered as part of the Lhasa Terrane (cf. Dewey et al., 1988; Xu et al., 1985; Yin and Harrison, 2000). However, we note that there is a distinct difference of age-probability distributions of detrital zircons of pre-Permian metasedimentary rocks from the Amdo basement (strong peaks at ~550 Ma and ~950 Ma; Guynn, 2006) and the Lhasa Terrane (strong peaks at ~540 Ma and ~1170 Ma; Zhu et al., submitted for publication-b), which likely indicate a different origin and therefore a different drift history between them. This, together with the presence of ophiolitic mélanges both south and north of the Amdo basement (Fig. 1b; Pan et al., 2004), results in an uncertainty in exploring the evolution history of the Amdo basement because the above difference requires further verification. Therefore, the Amdo basement is not involved in the following discussion. As discussed above, a back-arc basin (evolved to what is known as the Neo-Tethys south of the Lhasa Terrane) may have existed south of the central Lhasa subterrane microcontinent during the early Mesozoic in response to the southward subduction of the Bangong–Nujiang Tethyan Ocean seafloor (Fig. 5a). With this initial condition, the tectonomagmatic evolution of the Lhasa Terrane during the Mesozoic is best described as follows (Fig. 5):

(1) Crustal melting accompanying back-arc basin development (Fig. 5b–c): continued southward subduction of the Bangong–Nujiang Tethyan Ocean seafloor was accompanied by continued development of the back-arc basin towards the further development of the Neo-Tethyan Ocean. Emplacement (e.g., intrusion and/or underplating) of the subduction-related basaltic magmas contributed to the juvenile crust at the southern edge of central Lhasa subterrane (Fig. 5b–c). The basaltic magmas caused the crustal melting, producing hybrid melts with compositional diversity with varying mantle contributions in terms of zircon Hf isotopes as exemplified by the Late Triassic–Early Jurassic magmatic rocks in the southern and central Lhasa subterranes (Chu et al., 2006; Ji et al., 2009a; Liu et al., 2006; Yang et al., 2008; Zhang et al., 2007a, 2007b) (Figs. 5b, 6). This interpretation is geologically reasonable because (i) the central Lhasa microcontinent is narrow and was probably < 300 km wide at that time (Burg et al., 1983; Kapp et al., 2007); (ii) mantle contribution is also manifested by mafic enclaves (Table 1) in host granitoids from the central Lhasa subterrane. Continued southward subduction of the Bangong–Nujiang Ocean seafloor led to slab rollback at some time (Fig. 5c). This rollback then led to northward migration of magmatism to the northern Lhasa subterrane, as evidenced by the progressively younger magmatism from the central and southern Lhasa subterranes (started since as early as ~210 Ma) to the northern Lhasa subterrane (began as late as ca. 134 Ma) (Fig. 6).

(2) Initiation of northward subduction of the Neo-Tethyan Ocean seafloor as a response to the Lhasa–Qiangtang continental collision (Fig. 5d): Stratigraphy and sedimentology studies along the Bangong–Nujiang suture zone indicate that the Lhasa Terrane may have diachronously collided with the Qiangtang Terrane during the Cretaceous (earlier in the east and later in the west) (cf. Kapp et al., 2007; Yin and Harrison, 2000; Zhang et al., 2004). This continental collision may have triggered the northward subduction initiation (Niu et al., 2003) of the Neo-Tethyan Ocean seafloor towards beneath the southern Lhasa subterrane at its southern edge, subsequently generating subduction-related adakite-like rocks (~137 Ma; Zhu et al., 2009c) in the southern Lhasa subterrane (Fig. 5d). The absence of 150–140 Ma magmatism in the southern Lhasa subterrane (Ji et al., 2009a; Wu et al., 2010; this study), together with the decreasing mantle contribution (or increasing ancient crustal contribution) with time from ~145 to 120 Ma in the central Lhasa subterrane (Fig. 6) is consistent with the continued rollback of the Bangong–Nujiang Ocean seafloor subduction, which resulted in the northward migration of mantle magmatism and thus the emplacement of hybrid melts of more crustal (less mantle) contributions in the central Lhasa subterrane.

(3) Final Lhasa–Qiangtang amalgamation followed by the slab breakoff of the Bangong–Nujiang Tethyan Ocean floor subduction (Fig. 5e): Geochronological data show that the magmatism intensified at ~113 Ma (Fig. 2d) forming an along-strike linear zone in the central and northern Lhasa subterranes (Table 1; Zhu et al., 2009b, submitted for publication-a). Following our recent study on the Early Cretaceous magmatic rocks in the central Lhasa subterrane (Zhu et al., 2009b), we argue that the magmatic intensification with compositional diversity (Fig. 2a, b, c) may be caused by slab breakoff of the Bangong–Nujiang Tethyan Ocean floor subduction/underthrusting at that time (Fig. 5e). This is because contrasting behavior of oceanic (negatively buoyant) and continental (positively buoyant) portions of the same lithosphere will lead to slab breakoff after collision (von Blanckenburg and Davis, 1995; Wong et al., 1997). As a result, the slab breakoff would have caused localized asthenospheric upwelling and decompression melting. Such mantle-derived melt with mantle isotopic signatures will rise, intrude/underplate the overlying crust, as exemplified by the coeval mafic rocks (Kang et al., 2008; Liu et al., 2003; Zhang et al., 2004) and abundant dioritic enclaves (Zhu et al., 2009b) in Coqen and Xainza areas. In addition, the mantle-derived magmas may have also provided the heat and material for deep crustal anatexis, thus producing granitoid melts of isotopically hybrid compositions (Fig. 5e). Consequently, the mature crust-derived granitoid melts emplaced in the central Lhasa subterrane will have been assimilated by increased mantle-derived materials and thus have greater mantle isotopic signals at that time relative to the early granitoids in this subterrane, whereas the coeval juvenile crust-derived granitoid melts emplaced at the northern subterrane would have greater ancient crustal isotopic signals relative to the early granitoids in this terrane as observed (Fig. 6). The northern margin of the northern Lhasa subterrane may have shifted from an active continental margin into an intracontinental setting because of the absence of oceanic floor pull since ~113 Ma and subsequently experienced a southward obduction of elements from the Bangong–Nujiang suture zone and significant lithospheric/crustal thickening (Fig. 5f) during the Late Cretaceous to Paleocene (cf. Kapp et al., 2003, 2007; Murphy et al., 1997; Volkmer et al., 2007) driven by the ongoing northward subduction of the Neo-Tethyan Ocean floor beneath the southern Lhasa subterrane (Fig. 5f). Such a slab breakoff event marks a major change in the tectonic setting of the Lhasa Terrane, which is most likely controlled only by the northward subduction of the Neo-Tethyan Ocean floor since ~113 Ma and subsequent ridge subduction during the 100 to 80 Ma and normal steady subduction after 80 Ma beneath the southern Lhasa subterrane prior to the India–Asia collision in the early Cenozoic (Zhang et al., 2010a).

(4) Final India–Asia amalgamation followed by the slab breakoff of the Neo-Tethyan Ocean floor subduction: the intensified

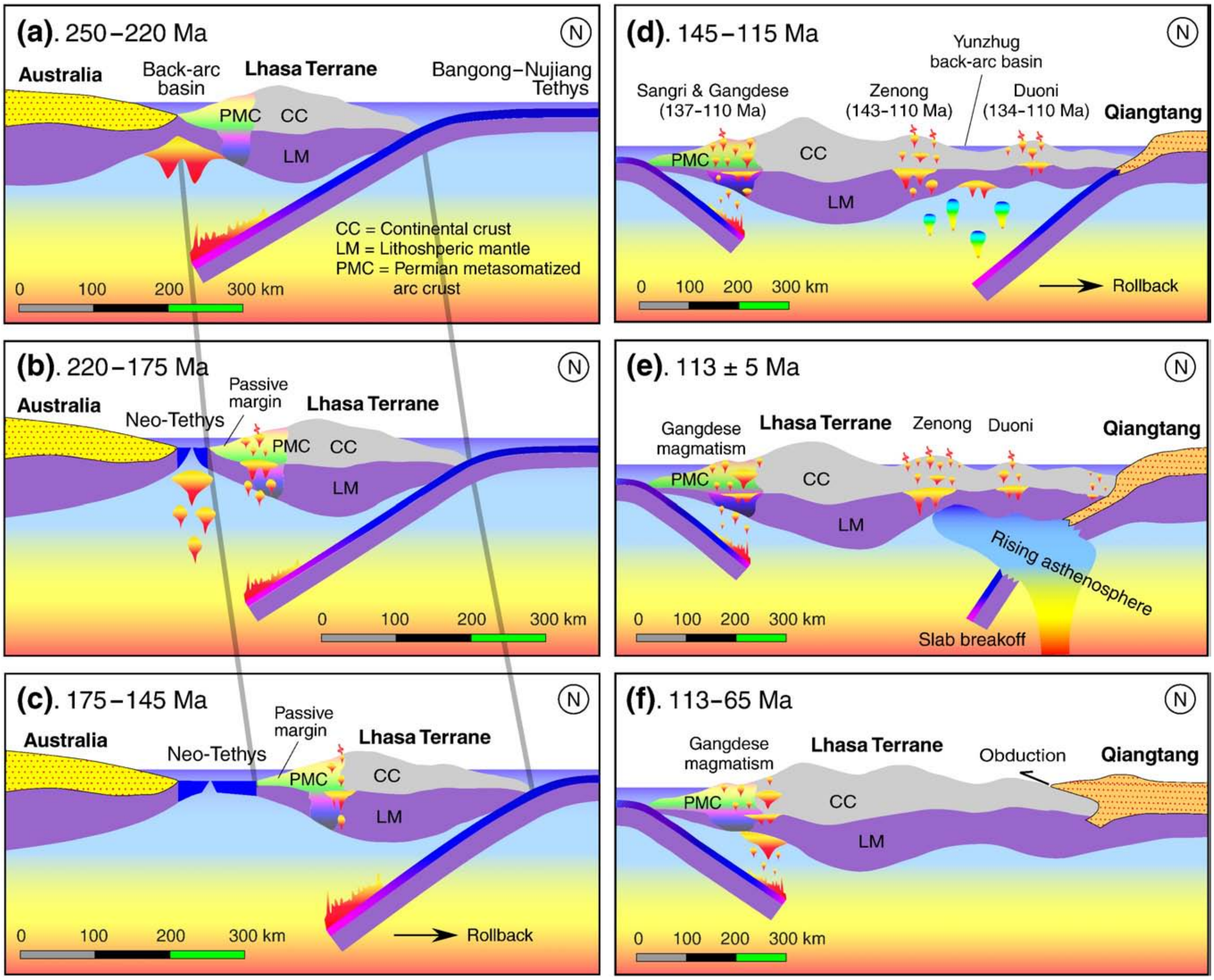

Fig. 5. Schematic illustrations of the nature and evolution of the Lhasa Terrane during the Mesozoic in terms of a series of north–south cross sections through time. This preferred model emphasizes that (i) the Neo-Tethyan Ocean opened as a back-arc basin (a, b, c), (ii) the northward subduction of the Neo-Tethyan Ocean seafloor may have initialized at the very Early Cretaceous (d), (iii) much of the Mesozoic magmatism in the Lhasa Terrane may be associated with the southward Bangong–Nujiang Tethyan Ocean seafloor subduction (b–e), and (iv) the northern margin of the Lhasa Terrane experienced a southward obduction of elements from the Bangong–Nujiang suture zone and significant lithospheric/crustal thickening since ~ 113 Ma (f). Note that the latitude scale range in a–c does not correspond to that in d–f. The Permian metasomatized arc crust is shown following Zhu et al. (2009a). See text for explanation.

magmatism with compositional diversity at ~52 Ma documented in the central part of the southern Lhasa subterrane have been attributed to the breakoff of the Neo-Tethyan Ocean floor (cf. Chung et al., 2009; Lee et al., 2009). We contend that the slab breakoff is a probable mechanism to account for (i) the narrow, linear zone of magmatism at ~52 Ma extended to the west near Hor (>1000 km long, E82° to E93° and <100 km wide) along the strike (Fig. 1b), and (ii) the increased input of ancient continental crust materials from the older rocks to the ~52 Ma rocks in the southern Lhasa subterrane (Fig. 6) because the rising asthenosphere followed by the slab breakoff is capable of causing anatexis of the adhering edge of the Indian continental lithosphere. Given the thermo-mechanical modeling suggestion that the most favorable time interval for slab breakoff is ~10–15 Myrs since the arrival of continental material at the trench (Macera et al., 2008), the slab breakoff at ~52 Ma would suggest the initial collisional contact between India and Asia at ~70–60 Ma. This reasoning and estimation is consistent with the general notion that the India–Asia collision took place in the timeframe of ~65–55 Ma (e.g., Chen et al., 2010; Chung et al., 2009; Ding et al., 2005; Lee and Lawver, 1995; Mo et al., 2003, 2007, 2008; Searle et al., 1987; Yin and Harrison, 2000;), but differs from other hypotheses that the collision began as late as early Oligocene (Aitchison et al., 2007) or ~43 Ma (Tan et al., 2010).

4.3. Crustal growth of the Lhasa Terrane

Previous studies highlight the importance of mantle contributions to the crust growth of the southern Lhasa subterrane since the Mesozoic in association with the Neo-Tethyan Ocean subduction and the India–Asia continental collision (e.g., Chung et al., 2009; Ji et al., 2009a; Mo et al., 2005b, 2007, 2008; Wu et al., 2010). New data reported here further signify such an important role of intrusion or underpalting of basaltic magmas in producing the juvenile crust of the southern Lhasa subterrane, as evidenced by the presence of mafic components, whether as microgranular enclaves, discrete plutons or andesites (Table 1), and the zircon Hf isotope data (Fig. 3). Obviously, in terms of zircon Hf isotopic compositions, the granitoids from the southern Lhasa subterrane are dominated by mantle contributions, up to 50–90% (Fig. 6). The "mantle" here and below refers to juvenile crust associated with recently subducted Tethyan ocean crust.

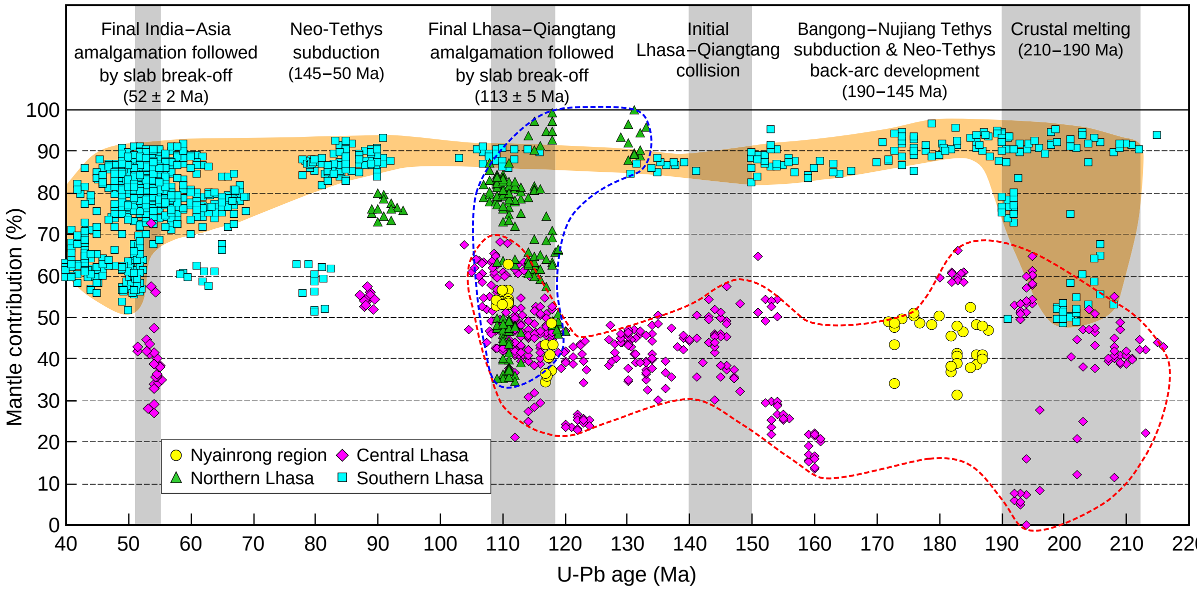

Fig. 6. Illustration of mantle contributions to the Mesozoic–early Tertiary magmatic rocks (Ji et al., 2009a; Zhu et al., 2009b, 2009c; this study) in terms of zircon Hf isotopes that changed with time and tectonomagmatic evolution of the Lhasa Terrane. The percentage of mantle contribution in the melt (assumed to be objectively recorded in the crystallized/crystallizing zircons) was calculated following Mišković and Schaltegger (2009). Note that one zircon with the most depleted Hf isotopic composition from a local basaltic andesite sample (sample YH06-3) is assumed to represent isotopically the pure composition of mantle-derived magma [$\varepsilon_{Hf}(t) = +18.8$, Hf = 8811 ppm], and one zircon with the most enriched Hf isotopic composition from a local strongly peraluminous granite (sample 08DX17) is considered as representing melts derived from mature continental crust of the Lhasa Terrane itself [$\varepsilon_{Hf}(t) = -20.5$, Hf = 12761 ppm]. The assumed end-members of binary mixing modeling are given in online supplementary material in Appendix A.

Similar juvenile crust formation and accretionary processes should have taken place in the northern Lhasa subterrane, where the Cretaceous volcanic rocks (andesite to rhyolite varieties) and granitoids that locally contain mafic micrgranular enclaves show positive zircon $\varepsilon_{Hf}(t)$ (Table 1; Zhu et al., submitted for publication-a). This points to a mantle-derived mafic magma contribution in the genesis of these rocks which can be explained in terms of mafic magma underplating as the result of the Bangong–Nujiang Tethyan Ocean seafloor subduction. As estimated by the zircon Hf isotopic compositions, the input of mantle material has contributed 30–100% to the formation of the magmatic rocks from the northern Lhasa subterrane (Fig. 6). The decreasing zircon $\varepsilon_{Hf}(t)$ towards the eastern part of the northern Lhasa subterrane reflects more ancient crustal (less mantle) contributions from the Lhasa microcontinent itself (and/or exotic Amdo basement and/or Qiangtang) in the generation of the granitoids (e.g., SB01-2).

The granitoids from the central Lhasa subterrane exhibit negative zircon $\varepsilon_{Hf}(t)$, ancient Hf isotope "crustal" model ages, and abundant inherited zircons (Fig. 3). These features, together with the contemporaneous presence of S-type and I-type melts (Fig. 2c), indicate that these rocks were largely derived from anatexis of mature continental crust materials. Nevertheless, the presence of mafic enclaves (Table 1), and wide spectrum of zircon $\varepsilon_{Hf}(t)$ of >10-ε units within a single sample (e.g., NML05-1, MB09-1, GRC02-1; Table 1) indicate that contributions from the mantle-derived magmas possibly related to magmatic underplating were involved in their generation (cf. Hawkesworth et al., 2010; Kemp et al., 2006; Niu, 2005). It is estimated that the mantle material input contributed 0–70% to the formation of the granitoids in terms of zircon Hf isotopic compositions (Fig. 6).

An accurate assessment of volume of magmatic addition to the crust of the Lhasa Terrane with time is not straightforward. This is because mantle-derived magmas may be arrested at major density interfaces, e.g., mantle/crust interface (Petford and Atherton, 1996), and because of erosion of magmatic rocks. However, if the surface outcrop area relates to magmatic productivity (cf. Kemp et al., 2009), then the widespread distributions of Early Cretaceous (Fig. 1b) and early Tertiary (cf. Lee et al., 2009; Mo et al., 2003, 2007, 2008) magmatic rocks with significant mantle input (Fig. 6) would indicate two significant periods of juvenile crust formation, represented, respectively, by Early Cretaceous magmatism associated with the Qiangtang–Lhasa collision in the northern Lhasa subterrane and by Early Tertiary magmatism associated with the India–Asia collision in the southern Lhasa subterrane. This emphasizes that processes associated with continental collision produce and preserve the juvenile crust, hence maintain the net continental crust growth (Hawkesworth et al., 2010; Mo et al., 2008; Niu and O'Hara, 2009).

5. Concluding remarks

A comprehensive dataset of bulk-rock geochemistry, zircon U–Pb geochronology and zircon Hf isotope geochemistry of the Mesozoic–early Tertiary magmatic rocks sampled along four north–south traverses across the Lhasa Terrane offers us an unprecedented understanding of the lithosphere architecture, the tectonic histories and crustal growth of the Lhasa Terrane in southern Tibet. These results represent added knowledge on the workings of the plate tectonics and have global geodynamic significance. Some key findings are summarized as follows:

1) The central Lhasa subterrane was once a microcontinent with Archean basement whereas the southern and northern portions are more recently accreted subterranes during its journey of drift across the Tethyan Ocean basins.
2) The Lhasa Terrane experienced continuous magmatism from the Late Triassic to early Tertiary (220–40 Ma) with two intense magmatic episodes culminated at ~113, and ~52 Ma that correspond to the present-day surface outcrop areas. The rocks emplaced during each of the two intense episodes are both compositionally diverse, ranging from metaluminous (I-type) to peraluminous (S-type) varieties.
3) The Bangong–Nujiang Ocean seafloor must have subducted southward beneath the northern Lhasa subterrane that likely began in the late Middle Permian (~263 Ma) and ceased in the late Early Cretaceous (~113 Ma), while the Neo-Tethyan Ocean

seafloor must have subducted northward beneath the southern Lhasa subterrane that likely initialized in the very Early Cretaceous. The former can account for much of the Mesozoic magmatism in the Lhasa Terrane.

4) The significant changes of zircon $\varepsilon_{Hf}(t)$ at ~113 and ~52 Ma record tectonomagmatic activities as a result of slab breakoff and related mantle melting events following the Qiangtang–Lhasa amalgamation and India–Lhasa amalgamation, respectively.
5) Significant mantle contribution to the crust formation in the Lhasa Terrane is represented, respectively, by Early Cretaceous magmatism associated with the Qiangtang–Lhasa collision in the northern Lhasa subterrane and by Early Tertiary magmatism associated with the India–Asia collision in the southern Lhasa subterrane. This ascertains the concept that processes associated with continental collision produce and preserve juvenile crust and hence maintains the net growth of continental crust.

Supplementary data associated with this article can be found, in the online version, at doi:10.1016/j.epsl.2010.11.005.

Acknowledgments

We are grateful for constructive reviews by Zeming Zhang, an anonymous reviewer, and editorial handling by Mark Harrison. This five-year research was financially co-supported by the Chinese National Natural Science Foundation (40830317, 40973026, and 40873023), the National Key Project for Basic Research of China (Project 2011CB403102, 2009CB421002, and 2006CB701402), the New Century Excellent Talents in University (NCET-10-0711), the Chinese 111 Project (No. B07011), and the programme of the Integrated Study of Basic Geology of Qinghai–Tibetan Plateau of the Chinese Geological Survey (1212010610104). Yaoling Niu thanks the Leverhulme Trust for a Research and Durham University for a Christopherson/Knott Fellowship. We also thank Yong-Sheng Liu, Hong-Lin Yuan for helping with LA-ICPMS U–Pb and Lu–Hf isotopic analyses, and Jian-Qi Wang, Hai-Hong Chen, Feng Yu, Liang-Liang Zhang for helping with whole-rock geochemical analysis.

References

Abbott, D.H., Drury, R., Mooney, W.D., 1997. Continents as lithological icebergs: the importance of buoyant lithospheric roots. Earth Planet. Sci. Lett. 149, 15–27.
Aitchison, J.C., Ali, J.R., Davis, A.M., 2007. When and where did India and Asia collide? J. Geophys. Res. 112, B05423.
Allègre, C.J., Courtillot, V., Tapponnier, P., et al., 1984. Structure and evolution of the Himalaya–Tibet orogenic belt. Nature 307, 17–22.
Audley-Charles, M.G., 1983. Reconstruction of eastern Gondwanaland. Nature 306, 48–50.
Audley-Charles, M.G., 1984. Cold Gondwana, warm Tethys and the Tibetan Lhasa block. Nature 310, 165–166.
Audley-Charles, M.G., 1988. Evolution of the southern margin of Tethys (North Australian region) from early Permian to late Cretaceous. Geol. Soc. Lond. Spec. Pub. 37, 79–100.
Baxter, A.T., Aitchison, J.C., Zyabrev, S.V., 2009. Radiolarian age constraints on Mesotethyan ocean evolution, and their implications for development of the Bangong–Nujiang suture, Tibet. J. Geol Soc 166, 689–694.
Burg, J.P., Proust, F., Tapponnier, P., Ming, C.G., 1983. Deformation phases and tectonic evolution of the Lhasa block (southern Tibet, China). Eclogae Geol. Helv. 76, 643–665.
Chen, Y.L., Zhang, K.Z., Li, G.Q., Nimaciren, Zhao, S.R., Chen, G.R., 2005. Discovery of an uniformity between the Upper Triassic Quehala Group and its underlying rock series in the central segment of the Bangong Co-Nujiang junction zone, Tibet, China. Geol. Bull. China 24, 621–624 (in Chinese with English abstract).
Chen, J.S., Huang, B.C., Sun, L.S., 2010. New constraints to the onset of the India–Asia collision: paleomagnetic reconnaissance on the Linzizong Group in the Lhasa Block, China. Tectonophysics. doi:10.1016/j.tecto.2010.04.024.
Chiu, H.Y., Chung, S.L., Wu, F.Y., Liu, D.Y., Liang, Y.H., Lin, Y.J., Iizuka, Y., Xie, L.W., Wang, Y.B., Chu, M.F., 2009. Zircon U–Pb and Hf isotope constraints from eastern Transhimalayan batholiths on the precollisional magmatic and tectonic evolution in southern Tibet. Tectonophysics 477, 3–19.
Chu, M.F., Chung, S.L., Song, B., Liu, D.Y., O'Reilly, S.Y., Pearson, N.J., Ji, J.Q., Wen, D.J., 2006. Zircon U–Pb and Hf isotope constraints on the Mesozoic tectonics and crustal evolution of southern Tibet. Geology 34, 745–748.
Chung, S.L., Chu, M.F., Ji, J.Q., O'Reilly, S.Y., Pearson, N.J., Liu, D.Y., Lee, T.Y., Lo, C.H., 2009. The nature and timing of crustal thickening in Southern Tibet: geochemical and zircon Hf isotopic constraints from postcollisional adakites. Tectonophysics 477, 36–48.
Coulon, C., Maluski, H., Bollinger, C., Wang, S., 1986. Mesozoic and Cenozoic volcanic rocks from central and southern Tibet: $^{39}Ar/^{40}Ar$ dating, petrological characteristics and geodynamical significance. Earth Planet. Sci. Lett. 79, 281–302.
DePaolo, D.J., Weaver, K.L., Mo, X.X., Zhao, Z.D., Harrison, T.M., 2008. Regional isotopic patterns in granitic rocks of southern Tibet and evolution of crustal structure during the Indo–Asian collision. Goldschmidt Conference Abstracts, p. A211.
Dewey, J.F., Shackelton, R.M., Chang, C.F., Sun, Y., 1988. The tectonic evolution of the Tibetan Plateau. Phil. Trans. R. Soc. Lond. A327, 379–413.
Ding, L., Kapp, P., Wan, X., 2005. Paleocene–Eocene record of ophiolite obduction and initial India–Asia collision, south-central Tibet. Tectonics 24, TC3001. doi:10.1029/2004TC001729.
Ferrari, O.M., Hochard, C., Stampfli, G.M., 2008. An alternative plate tectonic model for the Palaeozoic–Early Mesozoic Palaeotethyan evolution of southeast Asia (Northern Thailand–Burma). Tectonophysics 451, 346–365.
Flowerdew, M.J., Chew, D.M., Daly, J.S., Millar, I.L., 2009. Hidden Archaean and Palaeoproterozoic crust in NW Ireland? Evidence from zircon Hf isotopic data from granitoid intrusions. Geol. Mag. 146, 903–916.
Griffin, W.L., Wang, X., Jackson, S.E., Pearson, N.J., O'Reilly, S.Y., Xu, X., Zhou, X., 2002. Zircon chemistry and magma mixing, SE China: in-situ analysis of Hf isotopes, Tonglu and Pingtan igneous complexes. Lithos 61, 237–269.
Guynn, J.H., 2006. Age and tectonic evolution of the Amdo basement: Implications for development of the Tibetan Plateau and Gondwana paleogeography. Unpubl. PhD thesis, The University of Arizona.
Guynn, J.H., Kapp, P., Pullen, A., Gehrels, G., Heizler, M., Ding, L., 2006. Tibetan basement rocks near Amdo reveal "missing" Mesozoic tectonism along the Bangong suture, central Tibet. Geology 34, 505–508.
Harris, N.B.W., Inger, S., Xu, R., 1990. Cretaceous plutonism in central Tibet: an example of post-collision magmatism? J. Volcan. Geotherm. Res. 44, 21–32.
Hawkesworth, C.J., Dhuime, B., Pietranik, A.B., Cawood, P.A., Kemp, A.I.S., Storey, C.D., 2010. The generation and evolution of the continental crust. J. Geol. Soc. 167, 229–248.
He, Z.H., Yang, D.M., Zheng, C.Q., Wang, T.W., 2006. Isotopic dating of the Mamba granitoid in the Gangdese tectonic belt and its constraint on the subduction time of the Neotethys. Geol. Rev. 52, 100–106.
Hoskin, P.W.O., Schaltegger, U., 2003. In: Manchar, J.M., Hoskin, P.W.O. (Eds.), The Composition of Zircon and Igneous and Metamorphic Petrogenesis: Zircon, Reviews of Mineralogy and Geochemistry, 53, pp. 27–62.
Hu, D.G., Wu, Z.H., Jiang, W., Shi, Y.R., Ye, P.S., Liu, Q.S., 2005. SHRIMP zircon U–Pb age and Nd isotopic study on the Nyainqêntanglha Group in Tibet. Sci. China D 48, 1377–1386.
Hu, Z.C., Gao, S., Liu, Y.S., Hu, S.H., Chen, H.H., Yuan, H.L., 2008. Signal enhancement in laser ablation ICP-MS by addition of nitrogen in the central channel gas. J. Anal. At. Spectrom. 23, 1093–1101.
Ji, W.Q., Wu, F.Y., Chung, S.L., Li, J.X., Liu, C.Z., 2009a. Zircon U–Pb chronology and Hf isotopic constraints on the petrogenesis of Gangdese batholiths, southern Tibet. Chem. Geol. 262, 229–245.
Ji, W.Q., Wu, F.Y., Liu, C.Z., Chung, S.L., 2009b. Geochronology and petrogenesis of granitic rocks in Gangdese batholith, southern Tibet. Sci. China D 52, 1240–1261.
Jordan, T.H., 1988. Structure and formation of the continental lithosphere. J. Petrol. 11–37 Special Lithosphere Issue.
Kang, Z.Q., Xu, J.F., Dong, Y.H., Wang, B.D., 2008. Cretaceous volcanic rocks of Zenong Group in north-middle Lhasa block: products of southward subducting of the Slainajap Ocean? Acta Petrologica Sin. 24, 303–314 (in Chinese with English abstract).
Kapp, P., Murphy, M.A., Yin, A., Harrison, T.M., Ding, L., Guo, J.R., 2003. Mesozoic and Cenozoic tectonic evolution of the Shiquanhe area of western Tibet. Tectonics 22, 1029. doi:10.1029/2001TC001332.
Kapp, P., Yin, A., Harrison, T.M., Ding, L., 2005. Cretaceous–Tertiary shortening, basin development, and volcanism in central Tibet. GSA Bull. 117, 865–878.
Kapp, P., DeCelles, P.G., Gehrels, G.E., Heizler, M., Ding, L., 2007. Geological records of the Lhasa–Qiangtang and Indo–Asian collisions in the Nima area of central Tibet. Geol. Soc. Am. Bull. 119, 917–932.
Kemp, A.I.S., Hawkesworth, C.J., Paterson, B.A., Kinny, P.D., 2006. Episodic growth of the Gondwana supercontinent from hafnium and oxygen isotopes in zircon. Nature 439, 580–583.
Kemp, A.I.S., Hawkesworth, C.J., Collins, W.J., Gray, C.M., Blevin, P.L., EIMF, 2009. Isotopic evidence for rapid continental growth in an extensional accretionary orogen: the Tasmanides, eastern Australia. Earth Planet. Sci. Lett. 284, 455–466.
Kosarev, G., Kind, R., Sobolev, S.V., Yuan, X., Hanka, W., Oreshin, S., 1999. Seismic evidence for a detached Indian lithospheric mantle beneath Tibet. Science 283, 1306–1309.
Lee, T.Y., Lawver, L.A., 1995. Cenozoic plate reconstruction of Southeast Asia. Tectonophysics 251, 85–138.
Lee, H.Y., Chung, S.L., Lo, C.H., Ji, J.Q., Lee, T.Y., Qian, Q., Zhang, Q., 2009. Eocene Neotethyan slab breakoff in southern Tibet inferred from the Linzizong volcanic record. Tectonophysics 477, 20–35.
Leeder, M.R., Smith, A.B., Yin, J.X., 1988. Sedimentology, paleoecology and palaeoenvironmental evolution of the 1985 Lhasa to Golmud Geotraverse. Philos. Trans. R. Soc. Lond. Ser. A 327, 107–143.
Li, P.W., Gao, R., Cui, J.W., Guan, Y., 2004. Paleomagnetic analysis of eastern Tibet: implications for the collisional and amalgamation history of the Three Rivers Region, SW China. J. Asian Earth Sci. 24, 291–310.

Liu, D.Z., Tao, X.F., Ma, R.Z., Shi, H., Zhu, L.D., Hu, X. W., 2003. 1: 250, 000 geological report of Coqen County with geological map. Chengdu University of Technology, Chengdu, 163–183 (unpublished, in Chinese).

Liu, Q.S., Jiang, W., Jian, P., Ye, P.S., Wu, Z.H., Hu, D.G., 2006. The zircon SHRIMP U–Pb age and petrochemical and geochemical features of Mesozoic muscovite monzogranite at Ningzhong. Tibet. Acta Petrologica Sin. 22, 643–652 (in Chinese with English abstract).

Liu, Y.S., Hu, Z.C., Gao, S., Günther, D., Xu, J., Gao, C.G., Chen, H.H., 2008. In situ analysis of major and trace elements of anhydrous minerals by LA-ICP-MS without applying an internal standard. Chem. Geol. 257, 34–43.

Liu, Y., Gao, S., Hu, Z., Gao, C., Zong, K., Wang, D., 2010. Continental and oceanic crust recycling-induced melt-peridotite interactions in the Trans-North China Orogen: U–Pb dating, Hf isotopes and trace elements in zircons of mantle xenoliths. J. Petrol. 51, 537–571.

Macera, P.M., Gasperini, D., Ranalli, G., Mahatsent, R., 2008. Slab detachment and mantle plume upwelling in subduction zones: an example from the Italian South-Eastern Alps. J. Geodyn. 45, 32–48.

Matte, Ph., Tapponnier, P., Arnaud, N., Bourjot, L., Avouac, J.P., Vidal, Ph., Liu, Q., Pan, Y., Wang, Y., 1996. Tectonics of Western Tibet, between the Tarim and the Indus. Earth Planet. Sci. Lett. 142, 311–330.

McKenzie, D., Priestley, K., 2008. The influence of lithospheric thickness variation on continental evolution. Lithos 102, 1–11.

Meng, F.Y., Zhao, Z.D., Zhu, D.C., Zhang, L.L., Guan, Q., Liu, M., Yu, F., Mo, X.X., 2010. Petrogenesis of Late Cretaceous adakite-like rocks in Mamba from the eastern Gangdese, Tibet. Acta Petrologica Sin. 26, 2180–2192 (in Chinese with English abstract).

Metcalfe, I., 2010. Tectonic framework and Phanerozoic evolution of Sundaland. Gondwana Res. doi:10.1016/j.gr.2010.02.016.

Mišković, A., Schaltegger, U., 2009. Crustal growth along a non-collisional cratonic margin: a Lu–Hf isotopic survey of the Eastern Cordilleran granitoids of Peru. Earth Planet. Sci. Lett. 279, 303–315.

Mo, X.X., Zhao, Z.D., Deng, J.F., Dong, G.C., Zhou, S., Guo, T.Y., Zhang, S.Q., Wang, L.L., 2003. Response of volcanism to the India–Asia collision. Earth Sci. Front. 10, 135–148 (in Chinese with English abstract).

Mo, X.X., Dong, G.C., Zhao, Z.D., Zhou, S., Wang, L.L., Qiu, R.Z., Zhang, F.Q., 2005a. Spatial and temporal distribution and characteristics of Granitoids in the Gangdese, Tibet and implication for crustal growth and evolution. Geol. J. China Universities 11, 281–290 (in Chinese with English abstract).

Mo, X.X., Dong, G.C., Zhao, Z.D., Guo, T.Y., Wang, L.L., Chen, T., 2005b. Timing of magma mixing in the Gangdese magmatic belt during the India–Asia collision: zircon SHRIMP U–Pb Dating. Acta Geol. Sin. 79, 66–76.

Mo, X.X., Hou, Z.Q., Niu, Y.L., Dong, G.C., Qu, X.M., Zhao, Z.D., Yang, Z.M., 2007. Mantle contributions to crustal thickening during continental collision: evidence from Cenozoic igneous rocks in southern Tibet. Lithos 96, 225–242.

Mo, X.X., Niu, Y.L., Dong, G.C., Zhao, Z.D., Hou, Z.Q., Zhou, S., Ke, S., 2008. Contribution of syncollisional felsic magmatism to continental crust growth: a case study of the Paleogene Linzizong Volcanic Succession in southern Tibet. Chem. Geol. 250, 49–67.

Murphy, M.A., Yin, A., Harrison, T.M., Dürr, S.B., Chen, Z., Ryerson, F.J., Kidd, W.S.F., Wang, X., Zhou, X., 1997. Did the Indo–Asian collision alone create the Tibetan plateau? Geology 25, 719–722.

Nimaciren, Xie, Y.W., Sha, Z.L., Xiluolangjie, Qiangbazaxi, Peng, D.P., Gesangsuolang, Luosongzhandui, 2005. 1: 250, 000 geological report of Nagqu County with geological map. Xizang Institute of Geological Survey, Lhasa, 103–107 (unpublished, in Chinese).

Niu, Y., 2005. Generation and evolution of basaltic magmas: some basic concepts and a new view on the origin of Mesozoic–Cenozoic basaltic volcanism in eastern China. Geol. J. China Universities 11, 9–46.

Niu, Y., O'Hara, M.J., 2009. MORB mantle hosts the missing Eu (Sr, Nb, Ta and Ti) in the continental crust: new perspectives on crustal growth, crust–mantle differentiation and chemical structure of oceanic upper mantle. Lithos 112, 1–17.

Niu, Y., O'Hara, M.J., Pearce, J.A., 2003. Initiation of subduction zones as a consequence of lateral compositional buoyancy contrast within the lithosphere: a petrologic perspective. J. Petrol. 44, 851–866.

Pan, G.T, Ding, J., Yao, D.S., Wang, L.Q., 2004. Guidebook of 1: 1, 500, 000 geologic map of the Qinghai–Xizang (Tibet) plateau and adjacent areas 1–148 (Cartographic Publishing House, Chengdu, China).

Pan, G.T., Mo, X.X., Hou, Z.Q., Zhu, D.C., Wang, L.Q., Li, G.M., Zhao, Z.D., Geng, Q.R., Liao, Z.L., 2006. Spatial-temporal framework of the Gangdese Orogenic Belt and its evolution. Acta Petrologica Sin. 22, 521–533 (in Chinese with English abstract).

Pearce, J.A., Mei, H.J., 1988. Volcanic rocks of the 1985 Tibet Geotraverse: Lhasa to Golmud. Philos. Trans. R. Soc. Lond. Ser. A327, 169–201.

Petford, N., Atherton, M., 1996. Na-rich partial melts from newly underplated basaltic crust: the Cordillera Blanca bathloith, Peru. J. Petrol. 37, 1491–1521.

Quidelleur, X., Grove, M., Lovera, O.M., Harrison, T.M., Yin, A., Ryerson, F.J., 1997. The thermal evolution and slip history of the Renbu Zedong Thrust, southeastern Tibet. J. Geophys. Res. 102, 2659–2679.

Rowley, D.B., 1996. Age of initiation of collision between India and Asia: a review of stratigraphic data. Earth Planet. Sci. Lett. 145, 1–13.

Royden, L.H., Burchfiel, B.C., van der Hilst, R.D., 2008. The geological evolution of the Tibetan Plateau. Science 321, 1054–1058.

Scherer, E.E., Whitehouse, M.J., Münker, C., 2007. Zircon as a monitor of crustal growth. Elements 3, 19–24.

Searle, M.P., Windley, B.F., Coward, M.P., Cooper, D.J.W., Rex, A.J., Rex, D., Li, T.D., Xiao, X.C., Jan, M.Q., Thakur, V.C., Kumar, S., 1987. The closing of Tethys and the tectonics of the Himalaya. GSA Bull. 98, 678–701.

Sengör, A.M.C., 1979. Mid-Mesozoic closure of Permo–Triassic Tethys and its implications. Nature 279, 590–593.

Sengör, A.M.C., 1987. Tectonics of the Tethysides: Orogenic collage development in a collisional setting. Ann. Rev. Earth Planet. Sci. 15, 213–244.

Streckeisen, A.L., Le Maitre, R.W., 1979. A chemical approximation to the modal QAPF classification of the igneous rocks. Neues Jb Mineralog. Abh. 136, 169–206.

Tan, X.D., Gilder, S., Kodama, K.P., Jiang, W., Han, Y.L., Zhang, H., Xu, H.H., Zhou, D., 2010. New paleomagnetic results from the Lhasa block: Revised estimation of latitudinal shortening across Tibet and implications for dating the India–Asia collision. Earth Planet. Sci. Lett. 293, 396–404.

Tilmann, F., Ni, J., INDEPTHIII Seismic Team, 2003. Seismic imaging of the downwelling Indian lithosphere beneath central Tibet. Science 300, 1424–1427.

Volkmer, J.E., Kapp, P., Guynn, J.H., Lai, Q., 2007. Cretaceous–Tertiary structural evolution of the north central Lhasa Terrane, Tibet. Tectonics 26, TC6007 doi: 6010.1029/2005TC001832.

von Blanckenburg, F., Davis, J.H., 1995. Slab breakoff: a model for syncollisional magmatism and tectonics in the Alps. Tectonics 14, 120–131.

Wen, D.R., Liu, D.Y., Chung, S.L., Chu, M.F., Ji, J.Q., Zhang, Q., Song, B., Lee, T.Y., Yeh, M.W., Lo, C.H., 2008. Zircon SHRIMP U–Pb ages of the Gangdese Batholith and implications for Neotethyan subduction in southern Tibet. Chem. Geol. 252, 191–201.

Wong, A., Ton, S.Y.M., Wortel, M.J.R., 1997. Slab detachment in continental collision zones: an analysis of controlling parameters. Geophys. Res. Lett. 24, 2095–2098.

Wu, F.Y., Yang, Y.H., Xie, L.W., Yang, J.H., Xu, P., 2006. Hf isotopic compositions of the standard zircons and baddeleyites used in U–Pb geochronology. Chem. Geol. 234, 105–126.

Wu, F.Y., Ji, W.Q., Liu, C.Z., Chung, S.L., 2010. Detrital zircon U–Pb and Hf isotopic data from the Xigaze fore-arc basin: Constraints on Transhimalayan magmatic evolution in southern Tibet. Chem. Geol. 271, 13–25.

Xu, R.H., Schärer, U., Allègre, C.J., 1985. Magmatism and metamorphism in the Lhasa block (Tibet): a geochronological study. J. Geol. 93, 41–57.

Yang, Z.M., Hou, Z.Q., Xia, D.X., Song, Y.C., Li, Z., 2008. Relationship between western porphyry and mineralization in Qulong copper deposit of Tibet and its enlightenment to further exploration. Miner. Deposits 27, 28–36 (in Chinese with English abstract).

Yang, J.S., Xu, Z.Q., Li, Z.L., Xu, X.Z., Li, T.F., Ren, Y.F., Li, H.Q., Chen, S.Y., Robinson, P.T., 2009. Discovery of an eclogite belt in the Lhasa block, Tibet: a new border for Paleo-Tethys? J. Asian Earth Sci. 34, 76–89.

Yin, A., Harrison, T.M., 2000. Geologic evolution of the Himalayan Tibetan Orogen. Ann. Rev. Earth Planet. Sci. 28, 211–280.

Yin, J.X., Xu, J.T., Liu, C.J., Li, H., 1988. The Tibetan Plateau: regional stratigraphic context and previous work. Philos. Trans. R. Soc. Lond. Ser. A 327, 5–52.

Zhang, K.J., Xia, B.D., Wang, G.M., Li, Y.T., Ye, H.F., 2004. Early Cretaceous stratigraphy, depositional environments, sandstone provenance, and tectonic setting of central Tibet, western China. GSA Bull. 116, 1202–1222.

Zhang, H.F., Xu, W.C., Guo, J.Q., Zong, K.Q., Cai, H.M., Yuan, H.L., 2007a. Zircon U–Pb and Hf isotopic composition of deformed granite in the southern margin of the Gangdese belt, Tibet: evidence for early Jurassic subduction of Neo-Tethyan oceanic slab. Acta Petrologica Sin. 23, 1347–1353 (in Chinese with English abstract).

Zhang, H.F., Xu, W.C., Guo, J.Q., Zong, K.Q., Cai, H.M., Yuan, H.L., 2007b. Indosinian orogenesis of the Gangdese terrane: evidences from zircon U–Pb dating and petrogenesis of granitoids. Earth Sci. J. China Univ. Geosci. 32, 155–166.

Zhang, K.J., Zhang, Y.X., Li, B., Zhong, L.F., 2007c. Nd isotopes of siliciclastic rocks from Tibet, western China: constraints on provenance and pre-Cenozoic tectonic evolution. Earth Planet. Sci. Lett. 256, 604–616.

Zhang, Z.M., Zhao, G.C., Santosh, M., Wang, J.L., Dong, X., Shen, K., 2010a. Late Cretaceous charnockite with adakitic affinities from the Gangdese batholith, southeastern Tibet: evidence for Neo-Tethyan mid-ocean ridge subduction? Gondwana Res. 17, 615–631.

Zhang, X.R., Shi, R.D., Huang, Q.S., Liu, D.L., Cidan, S.L., Yang, J.S., Ding, L., 2010b. Finding of high-pressure mafic granulites in the Amdo basement, central Tibet. Chin. Sci. Bull. 55. doi:10.1007/s11434-010-4127-y.

Zhao, T.P., Zhou, M.F., Zhao, J.H., Zhang, K.J., Chen, W., 2008. Geochronology and geochemistry of the c. 80 Ma Rutog granitic pluton, northwestern Tibet: implications for the tectonic evolution of the Lhasa Terrane. Geol. Mag. 145, 845–857.

Zhou, C.Y., Zhu, D.C., Zhao, Z.D., Xu, J.F., Wang, L.Q., Chen, H.H., Xie, L.W., Dong, G.C., Zhou, S., 2008. Petrogenesis of Daxiong pluton in western Gangdese, Tibet: Zircon U–Pb dating and Hf isotopic constraints. Acta Petrologica Sin. 24, 348–358 (in Chinese with English abstract).

Zhu, J., Du, Y.S., Liu, Z.X., Feng, Q.L., Tian, W.X., Li, J.P., Wand, C.P., 2005. Mesozoic radiolarian chert from the middle sector of the Yarlung Zangbo suture zone, Tibet and its tectonic implications. Sci. China D 49, 348–357.

Zhu, D.C., Pan, G.T., Mo, X.X., Wang, L.Q., Liao, Z.L., Zhao, Z.D., Dong, G.C., Zhou, C.Y., 2006. Late Jurassic–Early Cretaceous geodynamic setting in middle–northern Gangdese: new insights from volcanic rocks. Acta Petrologica Sin. 22, 534–546 (in Chinese with English abstract).

Zhu, D.C., Pan, G.T., Wang, L.Q., Mo, X.X., Zhao, Z.D., Zhou, C.Y., Liao, Z.L., Dong, G.C., Yuan, S.H., 2008a. Tempo-spatial variations of Mesozoic magmatic rocks in the Gangdese belt, Tibet, China, with a discussion of geodynamic setting-related issues. Geol. Bull. China 27, 1535–1550 (in Chinese with English abstract).

Zhu, D.C., Pan, G.T., Chun, S.L., Liao, Z.L., Wang, L.Q., Li, G.M., 2008b. SHRIMP zircon age and geochemical constraints on the origin of Early Jurassic volcanic rocks from the Yeba Formation, southern Gangdese in south Tibet. Int. Geol. Rev. 50, 442–471.

Zhu, D.C., Mo, X.X., Niu, Y.L., Zhao, Z.D., Yang, Y.H., Wang, L.Q., 2009a. Zircon U–Pb dating and in-situ Hf isotopic analysis of Permian peraluminous granite in the Lhasa terrane, southern Tibet: implications for Permian collisional orogeny and paleogeography. Tectonophysics 469, 48–60.

Zhu, D.C., Mo, X.X., Niu, Y., Zhao, Z.D., Wang, L.Q., Liu, Y.S., Wu, F.Y., 2009b. Geochemical investigation of Early Cretaceous igneous rocks along an east–west traverse throughout the central Lhasa Terrane, Tibet. Chem. Geol. 268, 298–312.
Zhu, D.C., Pan, G.T., Zhao, Z.D., Lee, H.Y., Kang, Z.Q., Liao, Z.L., Wang, L.Q., Li, G.M., Dong, G.C., Liu, B., 2009c. Early Cretaceous subduction-related adakite-like rocks in the Gangdese, south Tibet: products of slab melting and subsequent melt-peridotite interaction? J. Asian Earth Sci. 34, 298–309.
Zhu, D.C., Mo, X.X., Zhao, Z.D., Niu, Y.L., Wang, L.Q., Chu, Q.H., Pan, G.T., Xu, J.F., Zhou, C.Y., 2010. Presence of Permian extension- and arc-type magmatism in southern Tibet: paleogeographic implications. GSA Bull. 122, 979–993.
Zhu, D.C., Zhao, Z.D., Niu, Y., Mo, X.X., submitted for publication–a. Bulk-rock geochemistry, zircon U–Pb age and Hf–O isotope of the Baingoin batholith in the northern Lhasa Terrane, Tibet: Implications for the Lhasa–Qiangtang collision.
Zhu, D.C., Zhao, Z.D., Niu, Y.L., Dilek, Y., Mo, X.X., Submitted for publication–b. The Lhasa Terrane in southern Tibet came from Australia.